OPTIMAL DESIGN OF THE ROBOTIC EXOSKELETON FOR HAND REHABILITATION

A THESIS SUBMITTED TO
THE GRADUATE SCHOOL OF NATURAL AND APPLIED SCIENCES
OF
ATILIM UNIVERSITY

BY

Mohammad Hassan GOL MOHAMMADZADEH

IN PARTIAL FULFILLMENT OF THE REQUIREMENTS
FOR
THE DEGREE OF DOCTOR OF PHILOSOPHY
IN
THE DEPARTMENT OF MODELING AND DESIGN OF ENGINEERING SYSTEMS (MAIN FIELD OF STUDY: MECHATRONICS ENGINEERING)

FEBRUARY 2019

Approval of the Graduate School of Natural and Applied Sciences, ATILIM University.

Prof. Dr. Ali KARA
Director

I certify that this thesis satisfies all the requirements as a thesis for the degree of Doctor of Philosophy in the Department of Modeling and Design of Engineering Systems (Main Field of Study: Mechatronics Engineering), ATILIM University.

Assoc. Prof. Dr. Ender KESKİNKILIÇ
Head of Department

This is to certify that we have read the thesis "OPTIMAL DESIGN OF THE ROBOTIC EXOSKELETON FOR HAND REHABILITATION" submitted by Mohammad Hassan GOL MOHAMMADZADEH and that in our opinion it is fully adequate, in scope and quality, as a thesis for the degree of Doctoral.

Asst.Prof.Dr. Kutluk Bilge ARIKAN
Co-Supervisor

Prof. Dr. Hulusi Bülent ERTAN
Supervisor

Examining Committee Members:

Prof. Dr. Hulusi Bülent ERTAN
Mechatronics Engineering Department, ATILIM University

Asst. Prof. Dr. Muhammad Umer KHAN
Mechatronics Engineering Department, ATILIM University

Asst. Prof. Dr. Hakan TORA
Aircraft Electrics & Electronics Dept., ATILIM University

Asst.Prof. Dr. Ali Emre TURGUT
Mechanical Engineering Department, METU

Asst.Prof. Dr. Masoud LATIFINAVID
Mechatronics Engineering Department, UTAA

Date: *15.02.2019*

I hereby declare that all information in this document has been obtained and presented in accordance with academic rules and ethical conduct. I also declare that, as required by these rules and conduct, I have fully cited and referenced all material and results that are not original to this work.

Name, Last Name: Mohammad Hassan GOL MOHAMMADZADEH:

Signature:

ABSTRACT

OPTIMAL DESIGN OF THE ROBOTIC EXOSKELETON FOR HAND REHBILITATION

GOL MOHAMMADZADEH, Mohammad Hassan

PhD, Department of Modeling and Design of Engineering Systems (Main Field of Study: Mechatronics Engineering)

Supervisor: Prof. Dr. Hulusi Bülent ERTAN

Co-Supervisor: Asst.Prof.Dr. Kutluk Bilge ARIKAN

February 2019, 81 pages

This thesis is a part of the research project which aims to design and implement a robotic hand rehabilitation system. The disabilities caused by the cerebral vascular accidents are hemiplegic. Therefore, the system is designed to make the impaired hand be driven by the exoskeleton. This system consists of a robotic hand exoskeleton which is synchronized with the visual stimulus software and the monitoring system for the activity of the mirror neuron system. Focus of this thesis is on optimizing the exoskeleton mechanism using a multi-objective cost function in terms of the forward and backward transmission angles and the desired kinematics. Mathematical models based on the multibody dynamics approach are used for the design and simulation purposes. In addition, the quasi-static models are utilized.

The passive torques in the joints of the human finger are modeled with the ordinary and fractional order mathematical terms. In the simulations, both the integer and the fractional order passive torques are implemented. The fractional order model is mainly used to represent the anomaly due to the spasticity. Two control strategies, namely the Proportional-Integral-Derivative (PID) and Feedback Error Learning (FEL) types are designed and evaluated with simulations to control the exoskeleton system during the

pinching motion. It is shown that the adaptive controller, FEL, copes with the fractional order passive torques better than the PID controller. It is shown that the inverse and direct quasi-static models are used to estimate the passive torques.

Keywords: Feedback error learning, Hand exoskeleton, Mechanism synthesis, Rehabilitation Robotic mirror therapy

ÖZ

EL REHABİLİTASYONU İÇİN GELİŞTİRİLEN HARİCİ İSKELETİN OPTİMAL TASARIMI

Mohammad Hassan GOL MOHAMMADZADEH
Doktora, Mühendislik Sistemlerinin Modellenmesi veTasarımı (MODES)
Tez Yöneticisi: Prof. Dr. Hulusi Bülent ERTAN
Ortak Tez Yôneticisi: Asst.Prof. Dr. Kutluk Bilge Arıkan
Şubat 2019, 81 sayfa

Bu tez çalışması, robotik el rehabilitasyon sistemi tasarım ve uygulamasını hedefleyen bir proje kapsamında gerçekleştirilmiştir. Beyin damarlarını etkileyen kazaların yol açtığı sakatlıklar hemiplejik olduğundan, projede işlev kaybı olan elin dış iskelet tarafından yönlendirildiği bir sistem üzerine yoğunlaşılmıştır. Bu çalışmada robotik harici iskelet, görsel uyaran yazılımı ve ayna nöron sistemi aktivitesini gözlemleyen ölçüm sistemi ile senkronize bir biçimde çalışmaktadır. Bu tez kapsamında harici iskelet mekanizmasının, ileri ve tersine aktarım açıları ve hedeflenen kinematiği kullanan bir çoklu amaç fonksiyonu ile eniyilenmesi hedeflenmiştir. Çoklu gövde dinamiği modelleri ve sanki-statik yapıdaki kinetik modeller, tasarım ve benzetim amaçlı geliştirilmiş ve kullanılmıştır.

Projemizde insan parmağının eklemlerindeki pasif torklar tam ve kesirli mertebe diferansiyel denklemlerle modellenmiştir. Parmağın dış iskelet ile bütünleşik benzetimlerinde tam ve kesirli mertebeden pasif torklar uygulanmıştır. Kesirli mertebe torklar, parmakta spastisite sonucu oluşan anomalinin modellenmesi için önerilmiştir. İnce kavrama hareketini sağlamak amacıyla PID ve FEL tipi denetimciler tasarlanmış ve model üzerinde sınanmıştır. Uyarlamalı bir kontrolcü olan FEL'in, kesirli mertebe pasif torklar etkin olduğunda PID'den daha başarılı sonuçlar verdiği gözlenmiştir. Direkt ve tersine sanki-statik modellerin, pasif torkların kestirimine yönelik kullanımı da tez kapsamında sunulmuştur.

Anahtar Kelimeler: Hata geri besleme ile öğrenme, Harici iskelet, Mekanizma sentezi, Rehabilitasyon, Robotik ayna terapisi.

To My Family

ACKNOWLEDGMENTS

I shall thank to all the academic and personnel staffs of the mechatronics and MODES departments of ATILIM University.

The financial support of The Scientific and Technical Research Council of Turkey (TUBITAK) is also acknowledged. This thesis study was supported by the Scientific and Technical Research Council of Turkey (TÜBİTAK) under the Grant 114E621 which is entitled as: "Investigation of the Mirror Neurons and Development of the Robotic Mirror Therapy System".

Finally, I thank my Co-Supervisor Dr. Kutluk Bilge ARIKAN for his supports during all the stages of my education.

TABLE OF CONTENTS

LIST OF TABLES

TABLES

LIST OF FIGURES

FIGURES

LIST OF SYMBOLS/ABBREVIATIONS

PIP	Proximal Interphalangeal joint
DIP	Distal Interphalangeal joint
MP/MCP	Metacarpophalangeal joint
VW	Virtual Work
EEG	Electroencephalography
ANN	Adaptive Neural Network
FEL	Feedback Error Learning
ALGA	Augmented Lagrangian Genetic Algorithm
RMS	Root Mean Square
DOE	Design of Experiments

CHAPTER 1

INTRODUCTION

In recent years the number of patients with hand disability as a result of a cerebral vascular accident or bone fracture has increased. A long-time insistent rehabilitation is needed to recover the functional losses. Shortage of therapists, long rehabilitation periods always makes it more difficult for patients to completely recover their lost abilities.

Many studies have been carried on the hand rehabilitation systems. For example Functional Electrical Stimulation (FES) [1, 2] is proved as a valuable tool for restoring of the hand functions. However, it is not a suitable approach for self-performing rehabilitation. The effectiveness of virtual reality-based stroke rehabilitations [3] has been proven for the hand rehabilitation. The rehabilitation robots serve to shorten the rehabilitation time and assist the therapists. Arm rehabilitation with the aid of a robot [4], is done by providing a bi-manual, mirror type patient-controlled therapeutic exercise. Still, for hand motions such as gripping and pinching, these therapies are imperfect. To improve the quality of life of patients with hand impairments, a rehabilitation system with multiple functions and fine motions is needed [5]. Additionally, monitoring the joint angle motions and finger stiffness is needed for hand rehabilitation. Some systems have been presented to measure finger joint motions [6, 7].

In this thesis, a robotic hand exoskeleton which is synchronized with the visual stimulus software and the monitoring system for the activity of the mirror neuron system is presented. Focus of this thesis is on optimizing the exoskeleton mechanism using a multi-objective cost function in terms of the forward and backward transmission angles and the desired kinematics. Mathematical models based on the multibody dynamics approach are used for the design and simulation purposes. In addition, the quasi-static models are utilized.

In addition, the passive torques in the joints of the human finger are modeled with the ordinary and fractional order mathematical terms. In the simulations, both the integer and the fractional order passive torques are implemented. The fractional order model is mainly used to represent the anomaly due to the spasticity. Two control strategies,

namely the Proportional-Integral-Derivative (PID) and Feedback Error Learning (FEL) types are designed and evaluated with simulations to control the exoskeleton system during the pinching motion. It is shown that the adaptive controller, FEL, copes with the fractional order passive torques better than the PID controller. It is shown that the inverse and direct quasi-static models are used to estimate the passive torques.

CHAPTER 2

LITERATURE SURVEY

A human hand may have 20 degrees of freedom (DOFs) in kinematic point of view. Particularly, all fingers have 4 DOFs. Index, middle, ring and little fingers have 3 joints for each. From the distal to end, the joints are: the distal interphalangeal (DIP), the proximal interphalangeal (PIP), and the metacarpophalangeal (MCP) joints. The DIP and PIP joints have flexion/extension DOF, but the MCP joints has both flexion/extension and abduction/adduction DOFs.

For the thumb, there are 3 joints and 4 DOFs. From the distal to end, the joints are: the interphalangeal (IP), the metacarpophalangeal (MCP) and the Carpometacarpal (CMC) joints. The IP and MCP joints have flexion/extension DOF, whereas CMC joint has both flexion/extension and abduction/adduction DOFs.

The hand exoskeletons (Exo-hands), or active hand orthoses are one kind of robotic hands. Respecting other kinds of robotic hands, an Exo-hand is an actively controlled mechanical system attached to the human hand so two systems has coupled movements. To design such systems, some critical concerns should be considered based on their applications.

Exo-hands could be categorized to 3 main groups, according to their applications:

- Rehabilitation exoskeletons;
- Haptic exoskeletons;
- Assistive exoskeletons.

Rehabilitation exoskeletons are tools for recovering the lost function of hand by performing exercises.

Haptic exoskeletons are attached to the human hand to track the human hand motions for controlling another device by applying force feedback to the user's hand.

As an example, FESTO Exo-Hand is shown in Figure 1.

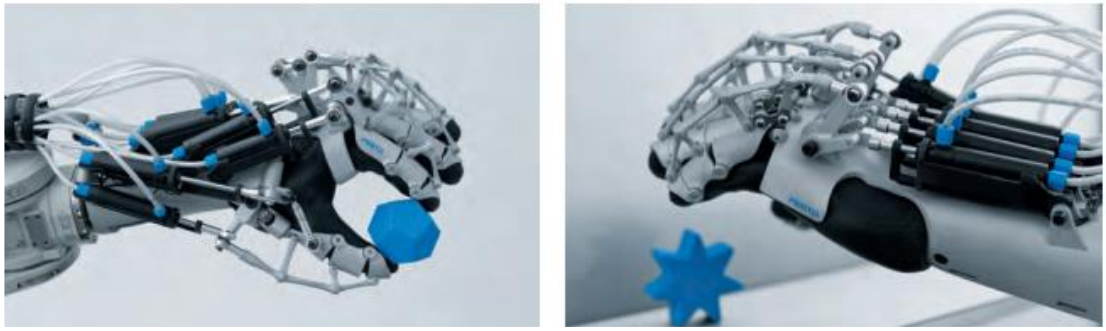

Figure 1: FESTO Exo-Hand

Assistive exoskeletons are devices that are used to help patients with hand disabilities to perform difficult or impossible activities in daily living with a supportive aid.

Considering any particular application, the designer must answer a wide range of questions, such as: the numbers of mechanism's DOFs (per single finger or whole hand), type and numbers of actuators, structural design of system, transmission system, control system etc.

The first issue that the designer must choose the numbers of mechanism's DOFs which is relative to the system kinematics. Considering the application of the exoskeleton, different numbers of DOFs can be used to move one or numbers fingers or the whole hand. Some exoskeletons couple the motion of DIP, PIP and MCP joints to move each finger or group of fingers (index, middle, ring and little ones) by 1 DOF or 2 DOFs. Whereas the control the hand can be done with up to 20 DOFs by 4 DOFs per single finger.

Other key factors to design the exoskeletons are the actuating and transmission systems. Various type of actuating and transmission system may be used. In some cases, pneumatic cylinders drive the links however many other devices are driven by electric motors. Typically, electric motors actuate exoskeleton joints by transmission systems like wire-driven mechanisms or linkage mechanisms.

Here, some of the similar systems are briefly presented.

This system in Figure 2 is composed of two main components: a hand rehabilitation system that controls the motion the index finger on paralyzed hand and a data glove connected to the healthy hand and provides the input data to control the rehabilitation system called "self-motion control" strategy or mirror therapy. The glove measures the angles of the MCP and PIP joints on the index finger of the healthy hand to feed the control input to the Exo-hand. A 2 DOFs exoskeleton mechanism controls the motion

of the injured finger by coupling the movement of the DIP and PIP joints. The exoskeleton is composed of 3 four-bar mechanisms which could be controlled by an actuator directly or indirectly such as a wire-driven mechanism or a connected linkage mechanism. The Tokyo university exoskeleton hand with its slave mechanism/ master data glove is shown in Figure 2 [8].

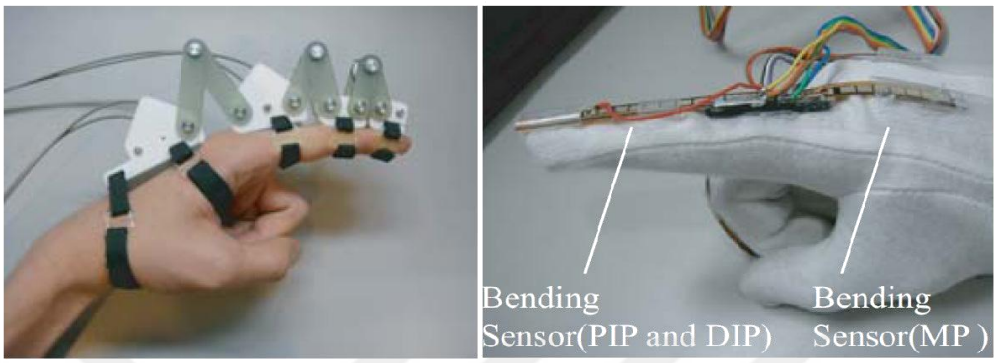

Figure 2: Tokyo University Exoskeleton Hand as slave and Data Glove as master

The Exoskeleton of Berlin University was designed to support the rehabilitation practice for injured hand of after stroke. The located Electromyography (EMG) sensors on palmer and dorsal side of the forearm controls the activities.

This mechanism has 20 DOFs with 4 active DOFs. For each finger: flexion/extension on MCP, PIP and DIP joints; abduction/ adduction on MCP joint. Also thumb has 4 DOFs. The CMC has movement of flexion/extension and abduction/adduction, while the MCP and IP joints has their own flexion motions. This Mechanism is shown in Figure 3 [9].

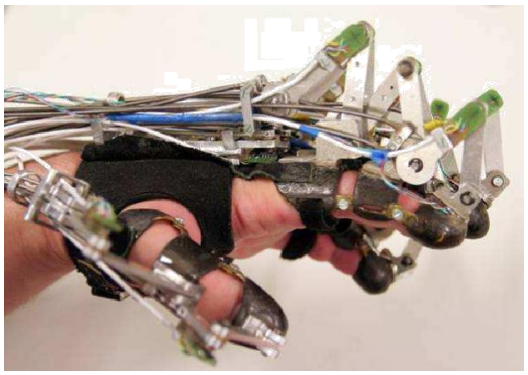

Figure 3: Berlin University Exo-Hand

This mechanism is designed for the rehabilitation of an incapacitated hand by self-motion control strategy or mirror therapy at the Gifu University. The system supports the motion of all fingers and thumb and assist the motion of the wrist. This Exo-hand has 18 DOFs for controlling human hand motion. Each finger has 3 DOFs, thumb has4

DOFs and the wrist 3 DOFs. The system controls the flexion/extension of MCP and PIP joints by using of 2 four-bar mechanisms actuating by 2 servo motors and provides the abduction/ adduction of MCP joint by another servomotor. Fixed impaired hand to the Exo-Hand by a glove of Gifu University Exo-Hand is shown in Figure 4 [10].

Figure 4: Fixed impaired hand to the Exo-Hand by a glove

This exoskeleton, shown in Figure 5, is designed for the rehabilitation process for patients with disability to control their hand after stroke by Milan University. The control system deeds EMG signals to control the motion of fingers. Using the measured EMG signals, the system can predict the target of motion and turns it into the patient's hand to execute it. On the pulley of each servomotor one potentiometers is placed to measure the rotational angle of the links.

This hand exoskeleton can control 2 DOFs of the human hand motion. The thumb motion is controlled with 1 DOF and the other 4 fingers are controlled with 1 DOF. All the flexion motions of the thumb and4 fingers are actuated with a wire-driven mechanism and two servomotors. So this Exo-hand is made of two under-actuated mechanisms [11].

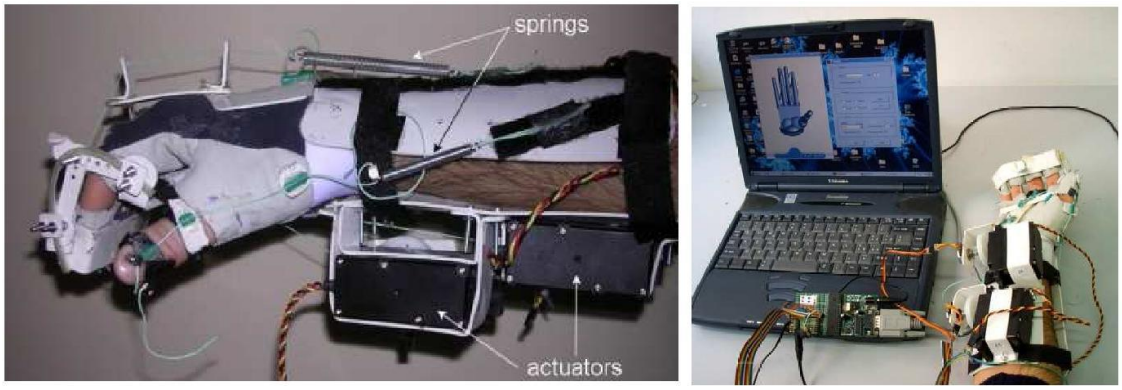

Figure 5: University of Milan Hand exoskeletons

The system, shown in Figure 6, was designed for the rehabilitation of pinching motion. The system deeds EMG signals for controlling motion of the patient's index finger.

This Exo-hand has 2 DOFs to repeat the flexion/extension motions of index finger. The motions of PIP and DIP are coupled together and MCP joint has own freedom. So flexion/extension motion of all joints are actuated and controlled by two pneumatic pistons. The index finger has another passive DOF for the abduction/adduction movement. Control of the exoskeleton motions is done by the user's EMG signals taking from biceps.

The exoskeleton doesn't have any position sensor to control the position of the finger joints, but for controlling the maximum forces exerted to the finger phalanges, the pistons are equipped with flexible pressure pneumatic regulators [12].

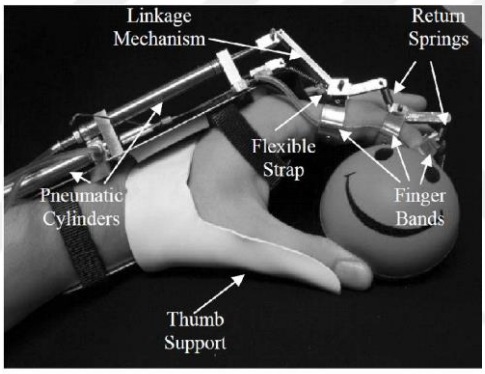

Figure 6: Exo-Hand of Pittsburgh University

The system in Figure 7 was designed for rehabilitation process of after stroke. By using an under-actuated mechanism, each finger the exoskeleton adapt itself generic shape of the grasped object. This Exo-hand controls 5 DOFs motions of the human's 5 fingers hand. The flexion/extension motions of DIP, PIP and MCP joints are controlled with a DC motor for each finger. The abduction/adduction motion of MCP is supported passively.

The main advantage of this under-actuated system is that the hand exoskeleton has its own ability of self-adaptation. The Finger mechanism of HANDEXOS and its slider-crack mechanism are shown in Figure 7 and Figure 8 [13].

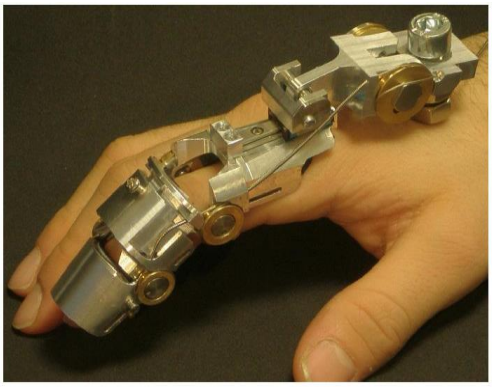

Figure 7: Finger mechanism of HANDEXOS

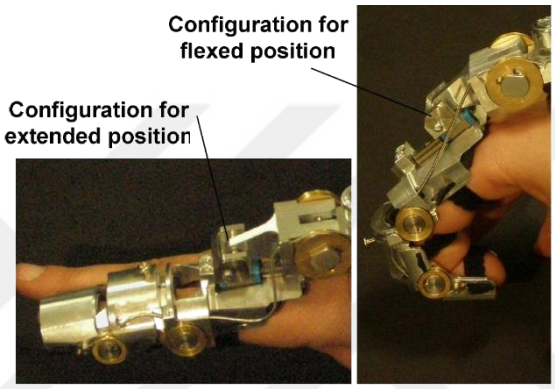

Figure 8: Slider-crack mechanism of HANDEXOS

This system, shown in Figure 9, is a rehabilitation system which is designed for the tendon repair therapy exercises. This exoskeleton is a 1 DOF mechanism attached to all finger phalanges for controlling the human index motion. The flexion/extension motions of DIP, PIP and MCP joints of index finger are controlled by 1 DOF, actuated with a single DC motor. The kinematics of the system is composed of a of five-bar mechanism (links: 1-5) and a four-bar mechanism (links: 4- 8) coupled together with 2 springs for constraining the mechanical limits.

The system is has different kinds of position sensors: potentiometers and encoder. Two potentiometers are instrumented at the joints coinciding with human PIP and DIP joints. Also, an optical encoder measures the position of the motor position. Three force sensors are located between the human finger and the exoskeleton. The controller is equipped with EMG electrodes to take the sample activity of muscles for evaluating the power-assist performance [14].

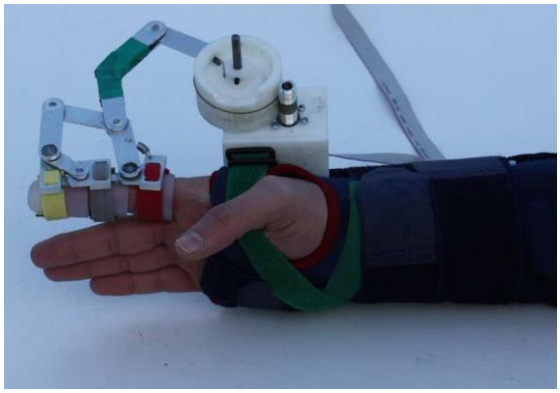

Figure 9: Finger Exoskeleton by SABANCI University

The design aim of this two finger exoskeleton is the haptic communication with a virtual reality environment system. The system cooperates with the human hand by exerting force on the fingertip which has 3 DOFs for the index finger and 3 DOFs for thumb finger. Each of them is actuated by 3 electrical motors, and wire-driven mechanism as a power transmission system. It is shown in Figure 10 [15].

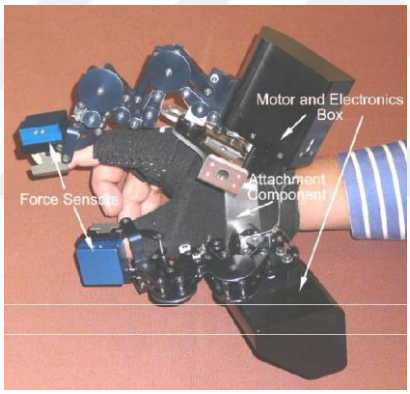

Figure 10: PERCRO Exo Hand I

DLR/HIT system has 1 DOF in each finger for all 5 fingers in a way that 3 six-bar mechanism are coupled to follow flexion/extension motion of PIP, DIP and MCP joints. One geared brushless motor with a reduction ratio 2:1, directly moves the first six-bar mechanism for flexion/extension motions of MCP. At the same time wires and adaptable slider mechanism moves MCP and PIP, and PIP and DIP, with a transmission ratio of 1:1.4 and 1.4:1 respectively [16]. The system is shown in Figure 11.

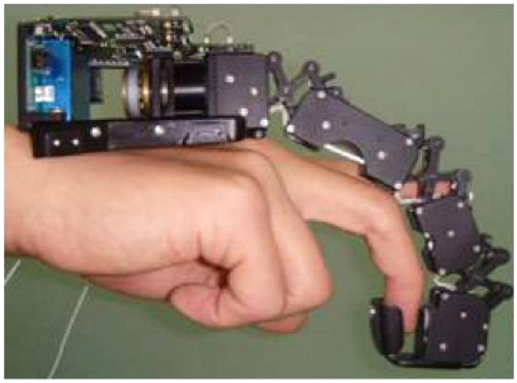

Figure 11: DLR/HIT Exo-Hand

The haptic system in Figure 12 is designed for virtual reality applications. The Exo-hand has 2 finger with 1 DOF in each of index and thumb finger. A 4-link serial mechanism controls flexion/extension motion of PIP, DIP and MCP joints of index finger. Two pulleys with the same radius couple the adduction and flexion of the thumb shown in Figure 12 [17].

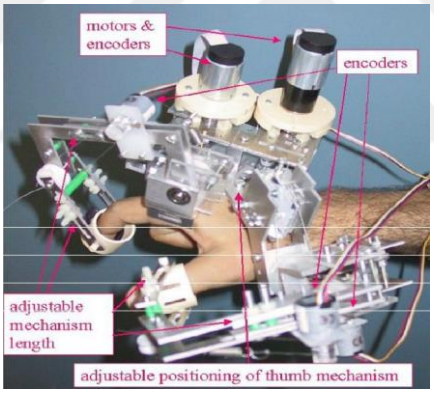

Figure 12: Robotics Center-Ecole des Mines de Paris Exo-Hand

This assistive in Figure 13 controls human hand and wrist motions. The exoskeleton assists 8 DOFs motions of human hand. The flexion/extension motion of index finger and the combination of middle, ring and little fingers are actuated with a 3 DOFs support system for each motions. The thumb motion is realized by 2 actuated DOFs [18] . The Exo-Hand of University of Tsukuba are shown in Figure 13 and Figure 14 which are taken from [25] and [18].

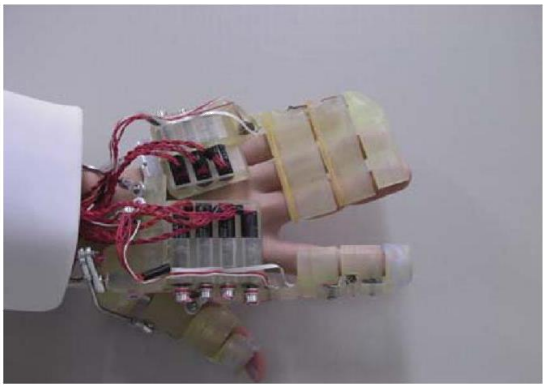

Figure 13: University of Tsukuba Hand Exoskeleton

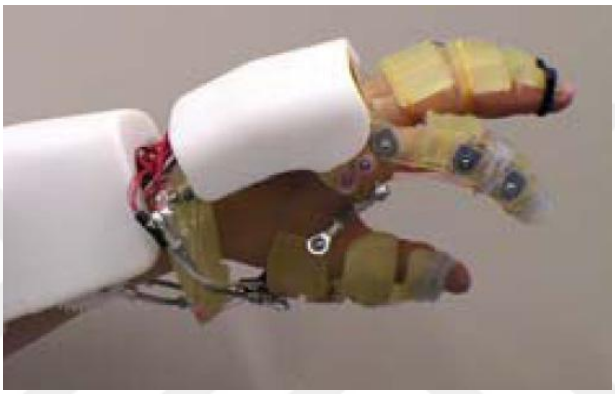

Figure 14: Pinching with the Exoskeleton of the University of Tsukuba

CHAPTER 3

ABOUT THE PROJECT

The major novelty of the project is to assess whether brain neuron activities during action observation and the execution of the actual motion generated by a robotic system can have an anticipatory effect on treatment of after stroke rehabilitation. For this purpose, a finger exoskeleton robot as a robot-induced technology for after-stroke rehabilitation, was used to give a completely synchronized pattern between action observations with execution in the experiments. So synchronizing of observation, robot execution and brain activity monitoring was a must. To overcome this challenge a trigger based system was designed to synchronize two PC's and three applications during each repetition in real time control, as shown in Figure 15.

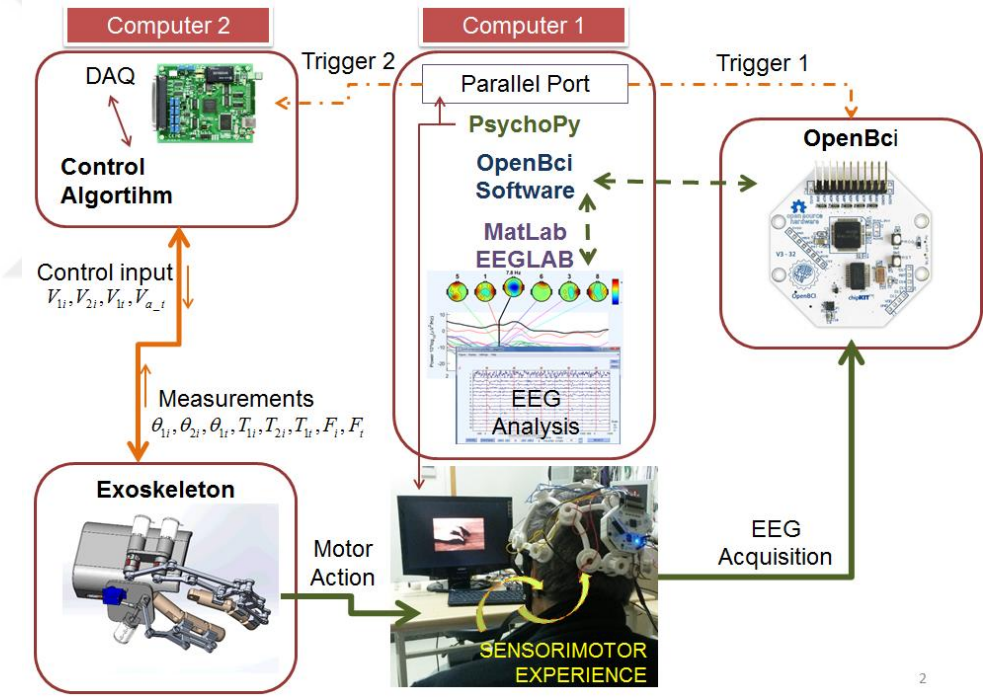

Figure 15: The schematic of the project

To test the synchronization of system for each repetition of the experiment, a real time trigger was sent to Open BCI and Simulink simultaneously from Psychophy.

The finger exoskeleton repeats the pinching action 4 times during 8 seconds, at the same time patient is observing a pre-saved motion of pinching action with the same pattern and the EEG is saved by Open BCI software. Thus, three software which are running on two PCs work synchronously.

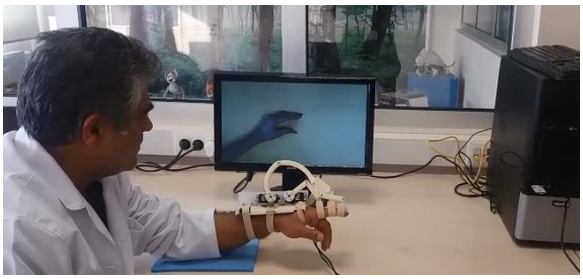

Figure 16: Synchronizing process of observation and execution of index finger

Showing each movie, at first frame trigger goes to high level in Psychophy and a trigger is sent to Simulink to run the Exo-robot with corresponding pattern. Similarly at the last frame of movie, trigger level becomes low.

For testing the system, the same scenario was repeated 35 times. All times were taken from real time running of system but only first repetition is shown in detail aşağıda in Figure 17.

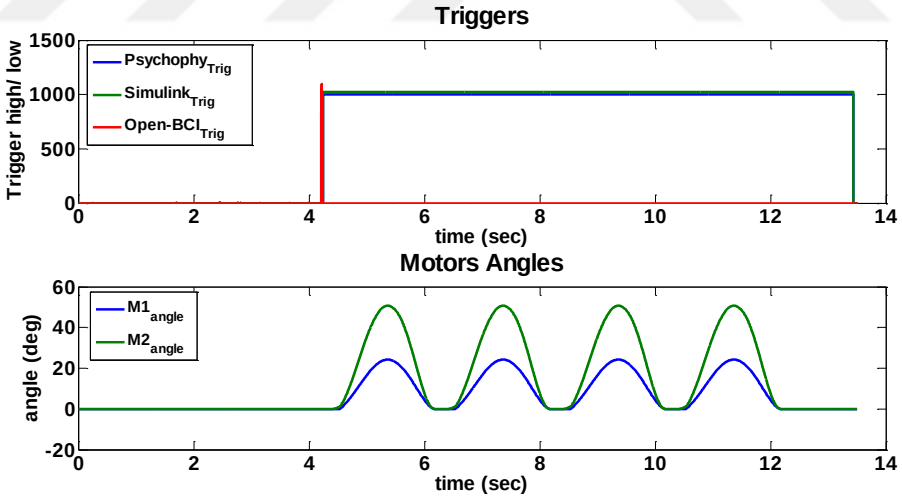

Figure 17: Time difference between Psychophy and Open BCI and Simulink.

The results show that the time difference between Psychophy and Simulink trigger is less than 5 milliseconds and the time difference between Psychophy and Open BCI trigger is less than 4 milliseconds. Considering monitor refresh frame rate as 15 milliseconds the synchronizing of triggers are acceptable.

CHAPTER 4

FINGER EXOSKELETON

During a hand rehabilitation, the therapists gives each finger joint flexion/extension motions independently within its movable range many times. So the need for an assistant device to give patient's hand such independent finger motions was realized.
To overcome this need in hand rehabilitation field, we developed an Exo-hand to assist in the flexion/extension of all the MP, PIP and DIP joints of index and thumb finger for rehabilitation purpose. In the design process, we took some other requirements into consideration, such as, safety, adoptability with different hand sizes and ease of attachment.
To address the safety concern, the movement range of joints and torque of the actuators should be carefully calculated so that the device does not cause any damage on patient's hand. In this manner some pre-experiments were done to understand the movement range of fingers in pinching action, determine the DOF of mechanism and the desired torque of actuators and designing the controller.

4.1 Human finger index finger motions

Human hand with its motor control is a complicated and multipurpose organic structure for handling of the environment. For understanding the hand functions, many biomechanical researches have been done. In most cases a human hand is typically modeled as a serial linkage mechanism which has 3 DOF's per finger, called DIP, PIP, MP joints, with flexion/extension and adduction/abduction motions as shown in Figure 18 [19].

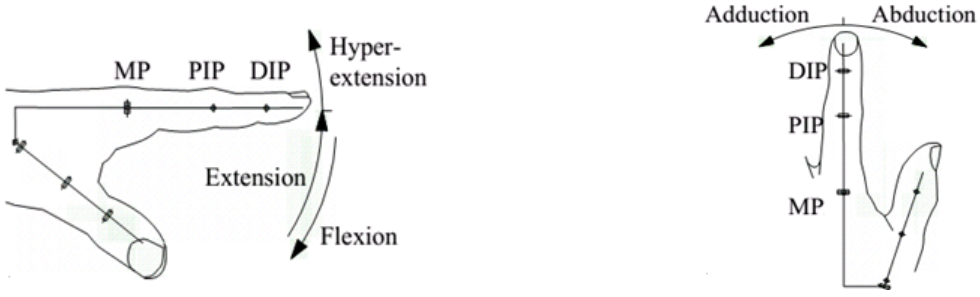

Figure 18: Human finger index finger motions

The MP has 2 DOF and is flexion/extension and adduction/abduction motion. But in this study we consider only flexion/extension and the joints are assumed to be precise revolute joints. To extract the pattern of human pinching, a study was done on 10 person male and female in the age range of 25-45. The pinching movements were recorded by Logitech HD Pro webcam C 920 from 45 cm distance. Later the recorded videos with 33.5 ms frame rate were analyzed by Tema TrackEye Motion 3.5 software. Human motion index finger during pinching, aptured by Tema-TrackEye is shown in Figure 19.

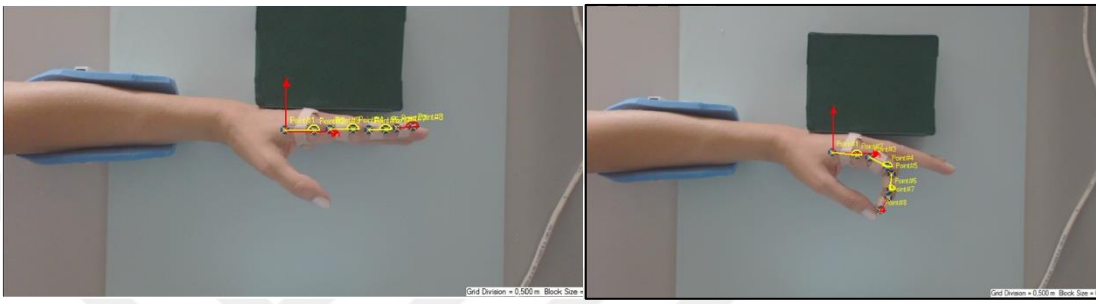

Figure 19: Captured Human motion index finger during pinching

The results of Tema-Motion analysis were normalized between 0-1 second. Then the trend-line of joints angles were defined by regression method on scattered graph as shown Figure 20, Figure 21 and Figure 22:

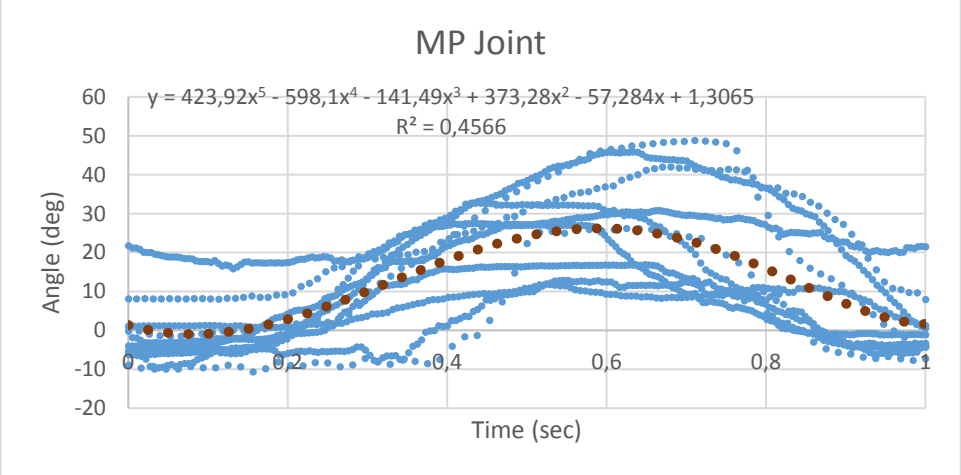

Figure 20: Scattered graph of MP joint movement of 10 subjects and the relative trend-line

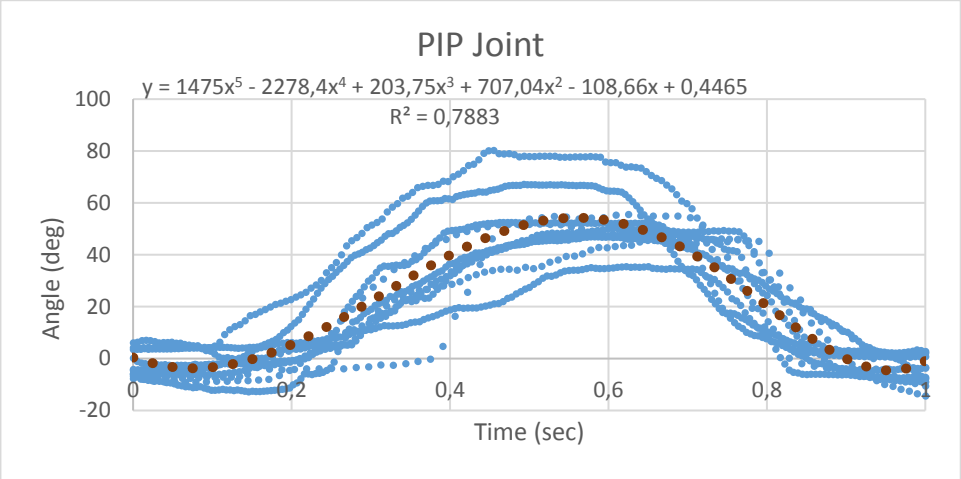

Figure 21: Scattered graph of PIP joint movement of 10 subjects and the relative trend-line

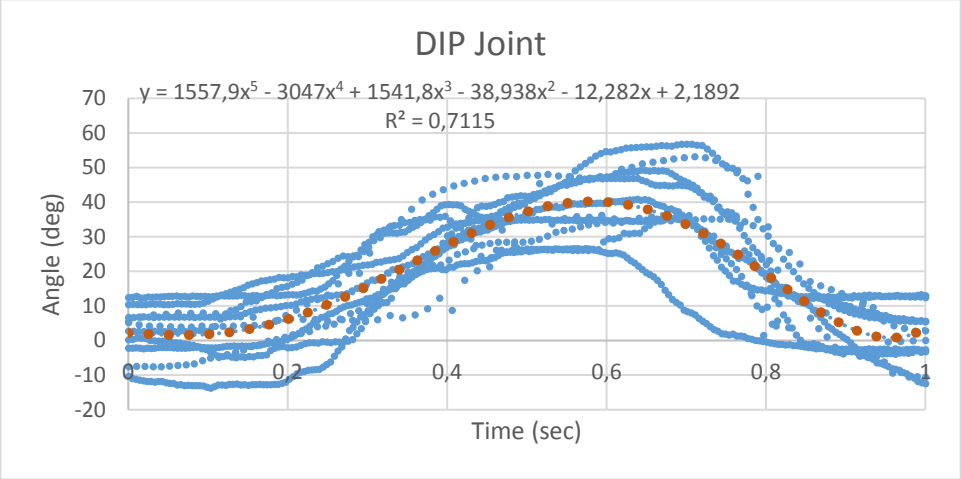

Figure 22: Scattered graph of DIP joint movement of 10 subjects and the relative trend-line

As shown on graphs the best fitted trend-lines for MP, PIP and DIP joint angles of 10 subjects, index fingers during pinching action are fifth order polynomial functions respectively as below.

$$\theta_{MP} = 423.92t^5 - 598.1t^4 - 141.49t^3 + 373.28t^2 - 57.284\,t + 1.3065$$

$$\theta_{PIP} = 1475t^5 - 2278.4t^4 + 203.75t^3 + 707.04t^2 - 108.66\,t + 0.4465$$

$$\theta_{DIP} = 1557.9t^5 - 3047t^4 + 1541.8t^3 - 38.938t^2 - 12.282\,t + 2.1892$$

The relation in movement between the PIP and DIP joints of index finger during pinching action for 10 subjects is extracted and shown in Figure 23.

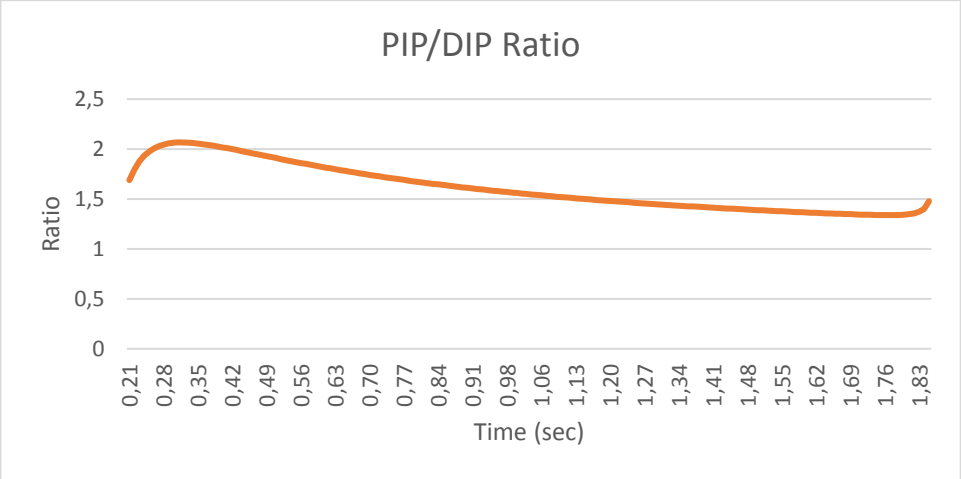

Figure 23: The relation between PIP-DIP joints motion of index finger during pinching action

This relation will be used later in Exo-hand design to couple the PIP-DIP joints motion in order to decrease the DOF's mechanism.

4.2 DOF of mechanism

For determining the DOF mechanism some experiments and simulation studies were done on non-human subjects. An exoskeleton system were designed and implemented to define the required of DOF of system.

The dimensions of exoskeleton is for the distal phalanx 26.8(mm) , medial phalanx 27(mm), proximal phalanx 50(mm) and metacarpal 80.1(mm). The mechanism has 10 number of total links and 12 number of total joints with three degree of freedom.

DOF= 3× (link-num-1) - (2×joint-num)

DOF= 3× (10-1) - (2×12) = 3 DOF

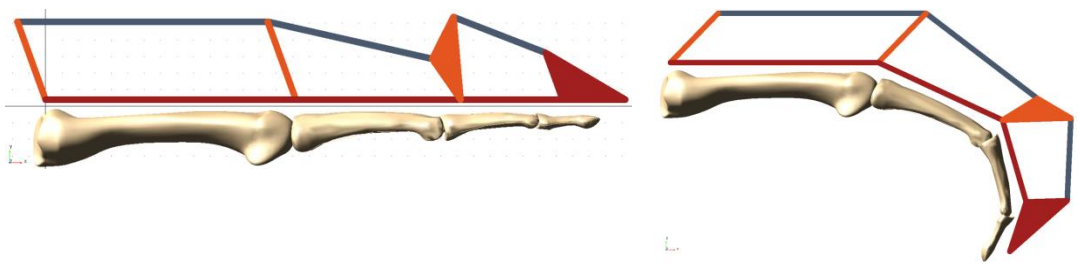

Figure 24: Exoskeleton system

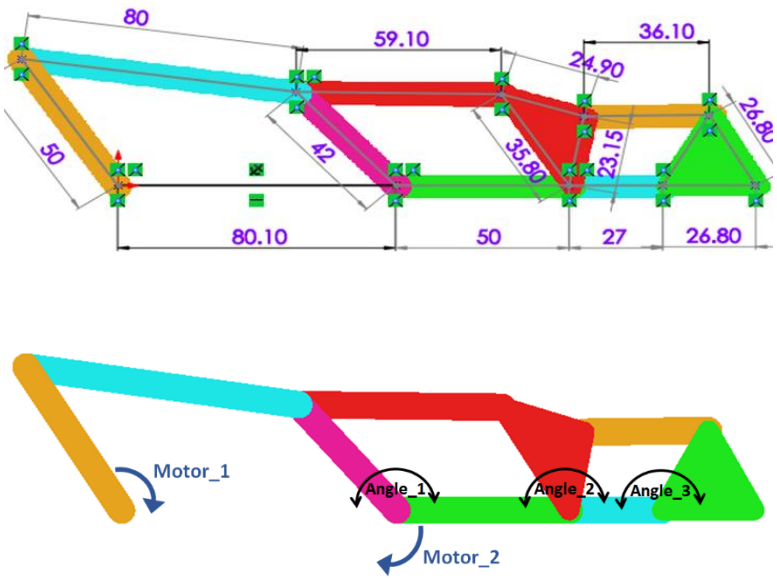

Figure 25: Top view of mechanism and reference angles in ADAMS View

Links are made of 3 mm and 5 mm thickness clear Acrylic Sheet - PLEXIGLASS SHEET (Nominal). This non-breakable, lightweight material can be cut, drilled, buffed, cemented, sanded, beveled, textured, formed, and painted. Links were designed and drawn in DWG format to be cut by laser cutting machine.

To achieve our purpose we tested two scenarios shown in Figure 26 and Figure 27.

- One actuated joint
- Two actuated joint

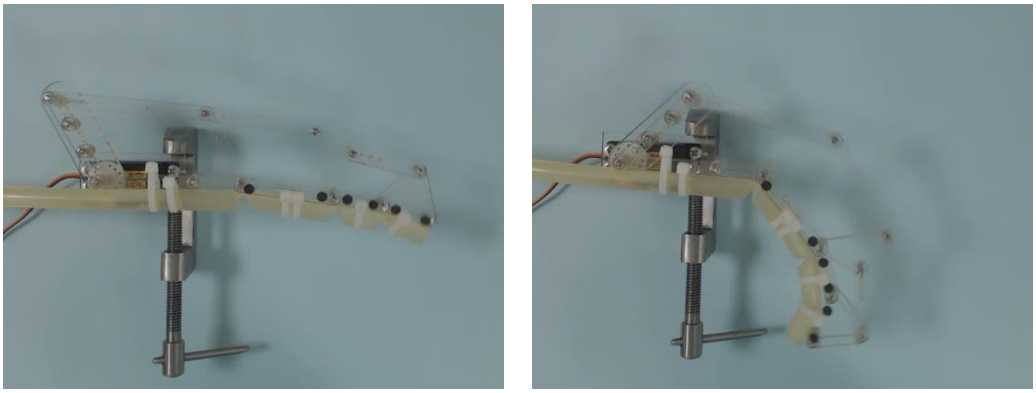

Figure 26: Top view of one actuated DOF mechanism

One actuated joint for a mechanism with three DOF's was not acceptable at all.

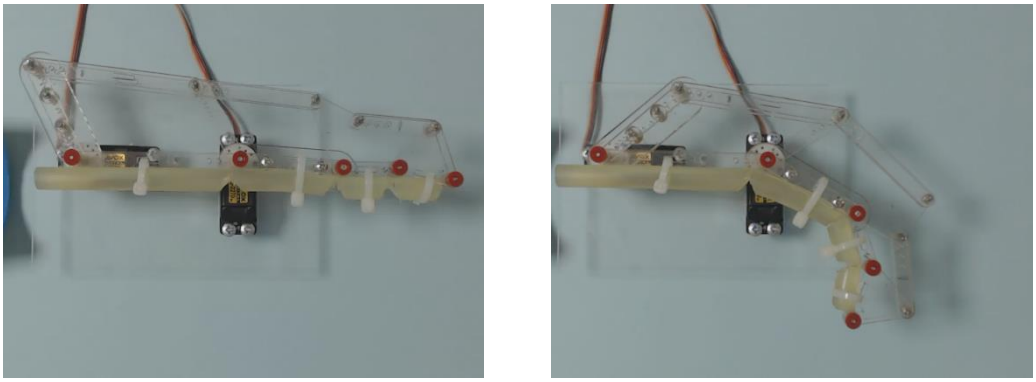

Figure 27: Top view of two actuated DOF mechanism

Two actuated joints for a mechanism with three DOF's was tested to determine whether it is acceptable or not. The controller was realized by Simulink model with a sample time of 0.1 second, shown in Figure 28, which sends the trajectory to the servo motors (HSR-5980SG HMI High Torque, Steel Gear Robot Servo) via a USB cable and Pololu Mini Maestro 12 channel servo controller at a Baud rate of 115200 bits/sec. It should be mentioned that servo motors have an inner closed loop controller with a sample time of millisecond. In this way we guarantee that all sending commands will be received and performed.

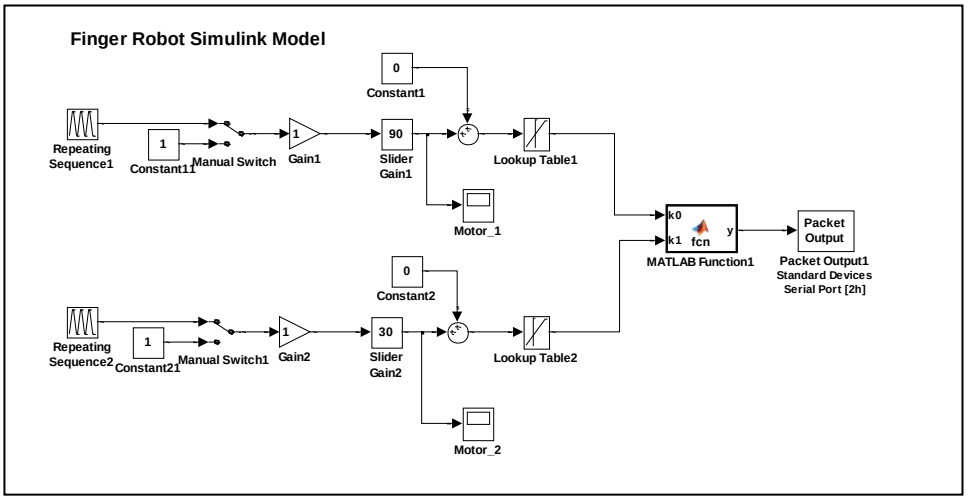

Figure 28: Matlab Simulink Model of real time control

4.3 Experiments and simulations results

The mechanism was tested with five different material having various stiffness's but the same input, then the movement of links was analyzed by TEMA Motion program to find out angles' variations.

Inputs: Motors Angles

The selected inputs implied on motor one and motor two is shown in Figure 29

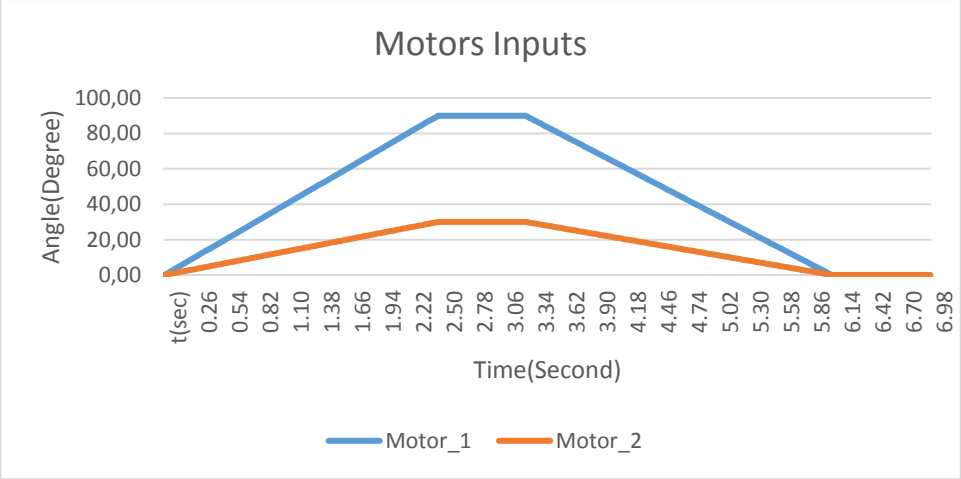

Figure 29: Motors inputs for implying desired motion on silicon finger

Outputs: Angles between Finger Links

The angle between metacarpal-proximal phalanx (MP) is defined as Angle 1, respectively the angle between proximal- medial phalanx (PIP) as Angle 2 and the angle between distal-medial phalanx (DIP) as Angle 3.

Angle 1 (MCP)

Angle 1 was directly driven by motor two so it is supposed to follow the exact pattern of input one. But as seen Figure 30, when the passive torque due to the stiffness is more than the stall torque of the motor, even Angle 1 is affected.

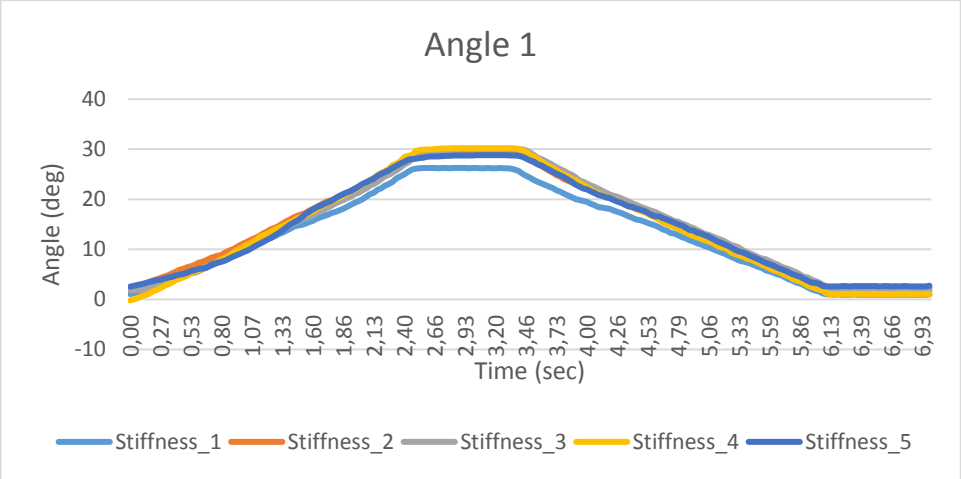

Figure 30: Joint MP angles for 5 different silicon fingers (experimental results)

Angle 2 and 3 (PIP/DIP)

These two angles are changed only by one input (motor 2), so the effect of stiffness is remarkable. As shown in Figure 31 and Figure 32, the differences between the patterns of different materials are remarkable.

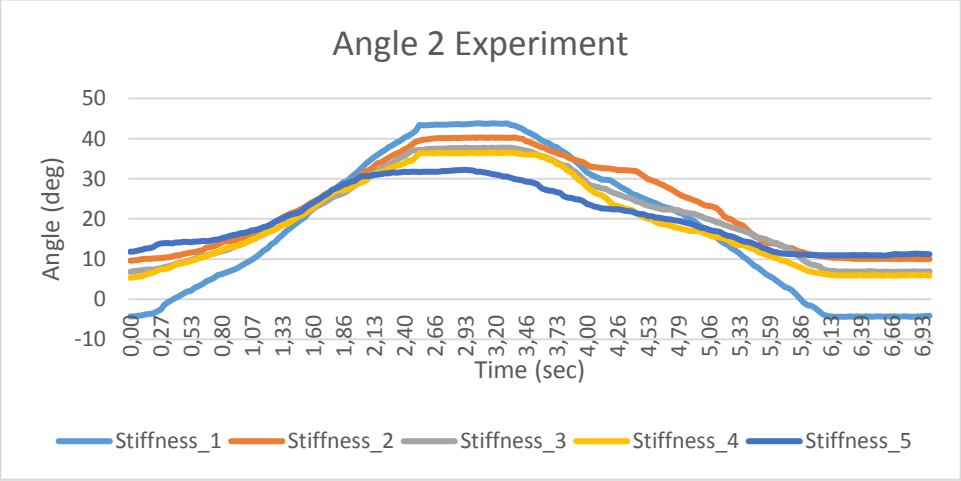

Figure 31: Joint PIP angles for 5 different silicon fingers (experimental results)

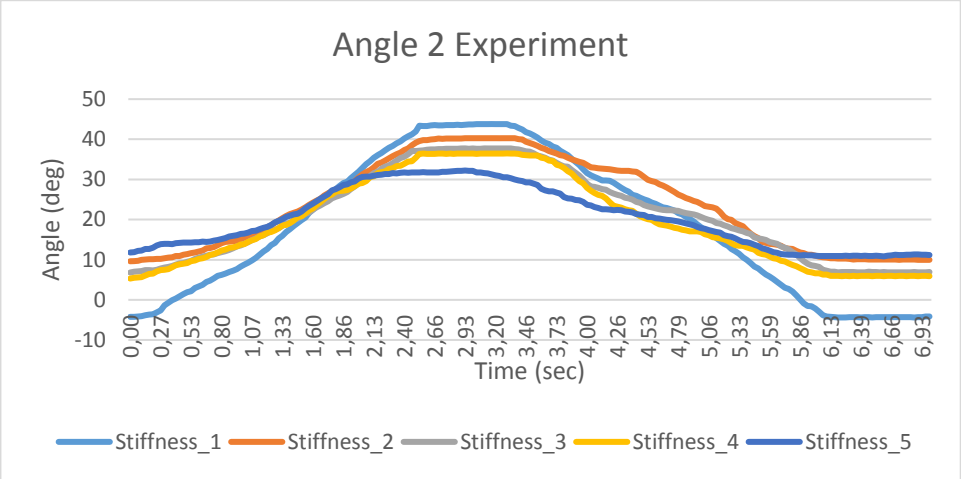

Figure 32: Joint DIP angles for 5 different silicon fingers (experimental results)

The same scenario was done by simulation in MSC Adams environment. To demonstrate the force asserted by finger on mechanism, two torsion springs with corresponding stiffness were defined on joint two and three (PIP and DIP). As previously done three different combination of stiffness applied on joint two and joint three and the angles were measured. The simulation results are shown in Figure 33 and Figure 34.

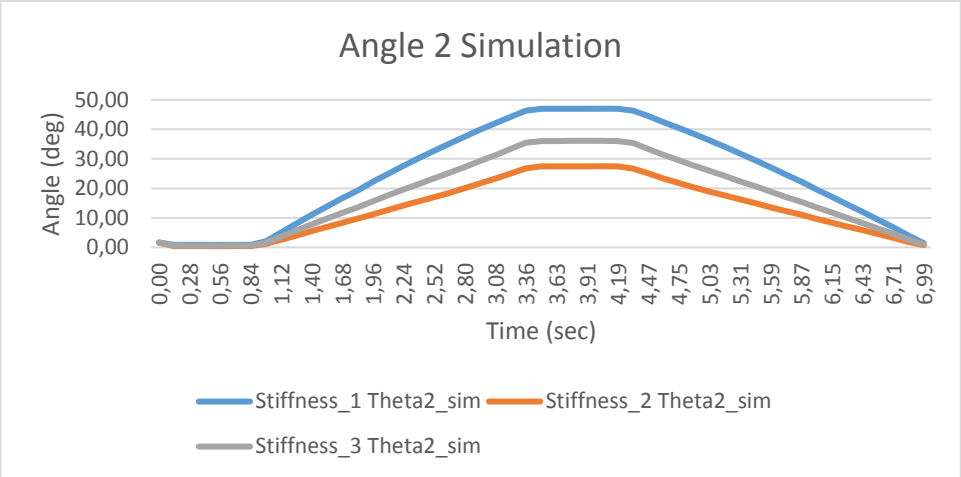

Figure 33: Joint PIP angles for 3 different stiffness (simulation results)

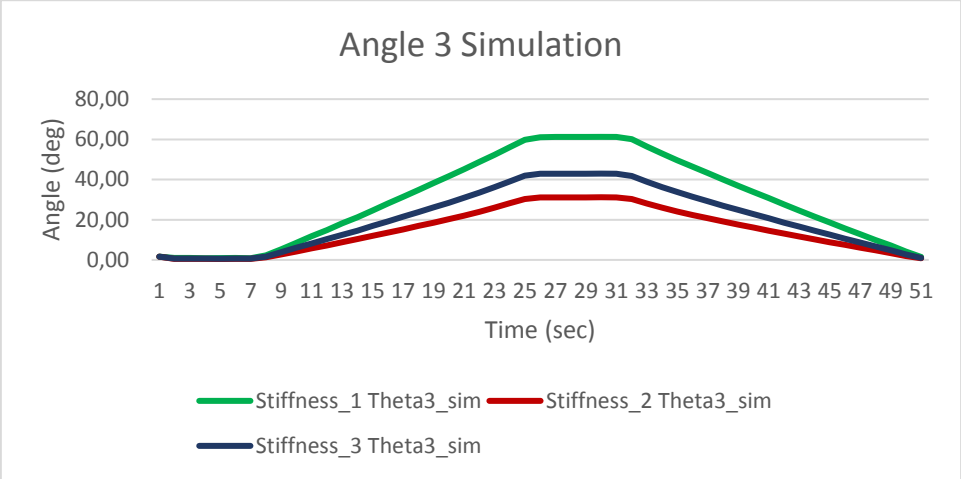

Figure 34: Joint DIP angles for 3 different stiffness (simulation results)

In both of the experimental and simulation results, the effect of stiffness can be obviously seen on the mechanism behavior. It was tried to estimate the stiffness of two joints in MSC Adams design evaluation tool in order to predict real mechanism behavior in simulation environment.

A rubber pipe was mounted on mechanism to play the role of finger and the previous experiments done again. The pattern of the Angle 2 and 3 were extracted. Optimization process was done for the pinching action.

Design of Experiments (DOE) was used for minimizing RMS (root mean square) of total difference between experimental angles and simulation angles as objective and stiffness_2 and stiffness_3 as design variables.

Total Difference =ABS ($\theta_{3\_Exp} - \theta_{3\_Sim}$) + ABS ($\theta_{2\_Exp} - \theta_{2\_Sim}$)

The DOE results for 400 trails are shown in Figure 35 and Table 1 :

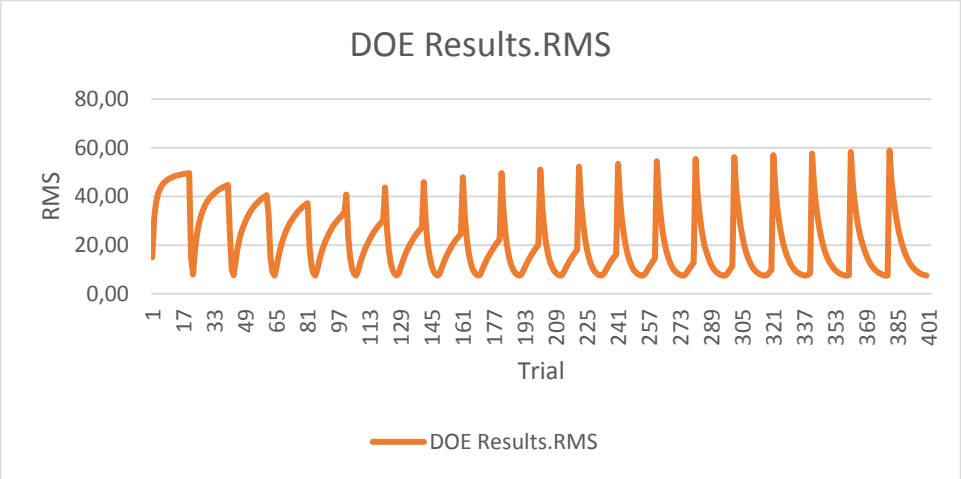

Figure 35: Optimization results for 400 trials

The obtained results are

RMS Maximum Value: 58.9069 (trial 381)

RMS Minimum Value: 7.45418 (trial 106)

Table 1: Minimum and maximum RMS among 400 trial

Result	Trial	RMS	stiffness_2	stiffness_3
Min	106	7.4542	1.3895	1.3895
Max	381	58.907	5.0000	0.10000

The simulation results for minimized RMS are shown in Figure 36 and Figure 37.

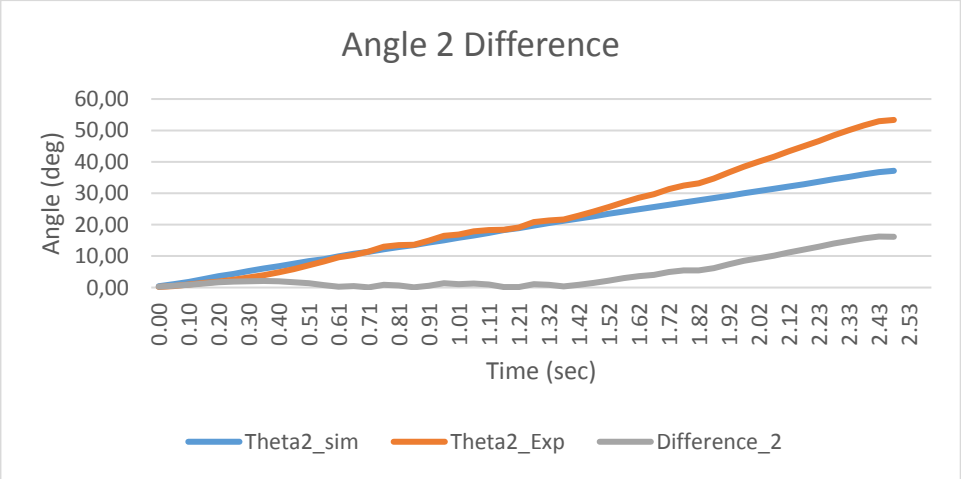

Figure 36: Simulation results of PIP joint for minimized RMS

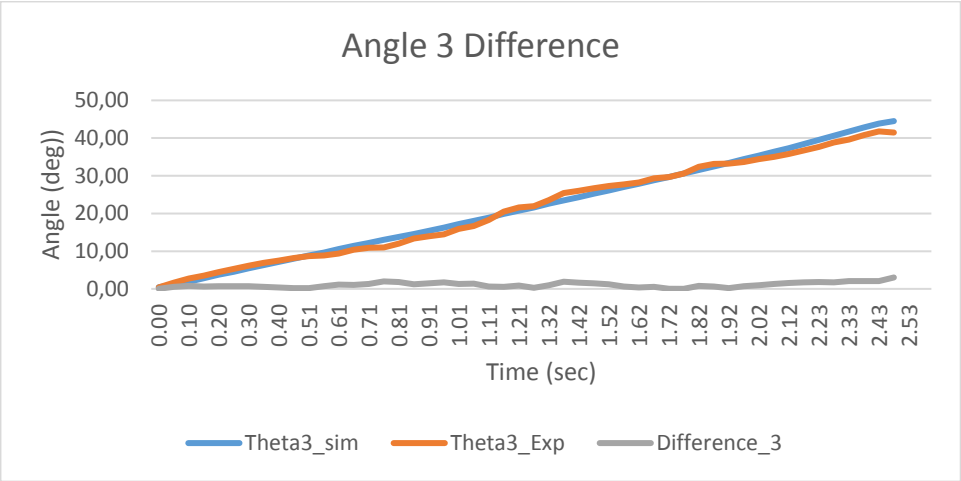

Figure 37: Simulation results of DIP joint for minimized RMS

In above graphs it is seen that difference between angle two (PIP) in experimental and simulation results is not constant and changes by angle. The results of these experiments leaded us to understand that, to follow the desired pattern exactly, the mechanism must be fully actuated without any passive joints.

CHAPTER 5

MECHANISM DESIGN

This thesis aims to design, fabrication and evaluation of an exoskeleton mechanism system of a finger rehabilitation robot. It can not only be used as a finger rehabilitation training tool after a stroke, but also to study the brain's recovery process during the rehabilitation therapy by monitoring the mirror neuron activities through EEG measurement.

The abstraction for this design problem is stated as: “Design an exoskeleton device for the human hand rehabilitation, in a way that the device is easy to control and exerts safely sufficient perpendicular forces on finger phalanges for pinching action, for using in medical therapy.” To achieve this, a biomechanical model of human finger was designed to drive MP and PIP joint directly , since the DIP joint moves indirectly together with the PIP joint [20], We used the relationship between PIP and DIP joints, found before, to control mechanism in a way that moves DIP joint moves in a desired trajectory.

5.1 Human finger characteristics

Length used in modeling of human finger is shown in Table 2 based on the a study on a biomechanically feasible extrinsic flexors [21].

Table 2: length of model segments based on human finger segments

Finger segment	Length (SD) (cm)	Model Length (cm)
Metacarpal	-	8
Distal	2.4(0.1)	2.5
Middle	3.1(0.2)	3
Proximal	4.9(0.3)	5

Such as considered in modeling the index finger of a clinician study [22], finger bodies were approximated by cylinders with circular cross sections so the geometrical and mass properties of the model segments have been summarized in Table 3.

Table 3: Geometrical and mass properties of the model segments based on human finger segments

Finger segment	Mass(kg)	I_{xx} (kgm2)	I_{yy}=I_{zz}(kgm2)
Distal	0.0054	6.7e-8	2.4e-6
Middle	0.0011	5e-9	1.6e-7
Proximal	0.0004	8e-10	3.5e-8
Metacarpal	0.016	3.9e-7	4.1e-6

5.2 Design requirements

The system should be capable for exerting desired torque or more on finger joints, by exerting forces perpendicularly on finger phalanges.

The device should be adept to be mounted on dorsal side of hands with an average size. The mechanism has 2 DOFs for each index and thumb finger, index and thumb closure with the exoskeleton. Finally, mechanism should have back-drivability and ease of control. An important design parameter is the required perpendicular force on the finger phalanges during flexion and extension to exert desired torque on finger joints. Table 4 shows healthy human index finger torques during flexion and extension movement [23].

Table 4: human index finger torques during flexion and extension movement

Joint	Motion	Male [Nm]	Female [Nm]
MP	Flexion	2.05	1.20
	Extension	1.30	0.55
PIP	Flexion	0.95	0.55
	Extension	0.6	0.45
DIP	Flexion	0.70	0.35
	Extension	0.35	0.15

During a rehabilitation process, therapists mostly pay attention to the amount of exerted forces on the patient's fingers for extension /flexion. The maximum safe joint torques to extension/flection determined by therapists, are measured by using a torque gauge as a substitute for a patient finger. As a results of these measurements, the acceptable torque for a hand supporting system are summarized in Table 5 [20].

Table 5: Acceptable torque for fingers as estimated by therapists' experiments

Joint	Motion	Thumb [Nm]	Index [Nm]
MP	Flexion	1.30	2.47
	Extension	2.60	2.93
PIP	Flexion	-	-
	Extension	-	2.87
DIP	Flexion	2.23	1.77
	Extension	2.48	1.97

5.3 Design process

"The four-bar mechanism is a very versatile linkage, which has been used extensively in a variety of machines, e.g. the Ackerman steering mechanism in automobiles, sewing machines, earth movers, packaging machines, automobile suspensions etc. Furthermore, Points on the coupler of a four-bar mechanism follow fascinating paths of order six (6-degree curves). This property is exploited to materialize designs pertaining to path generation. Given any arbitrary closed path, the objective then is to come up with a four-bar mechanism that can generate this path as a coupler curve.

We shall deal with a special class of four-bar mechanisms which satisfy the Grashoff's criterion. Crank-rocker type and crank-crank type mechanisms that fall in this category shall be used for the generation of closed coupler curves." [23]

To meet the requirements above a fully actuated 2 DOF mechanism is designed consisting of 4 four-bar loops in a way that two actuators drive the MP and PIP directly and DIP is driven indirectly related with PIP.

Regarding flexibility, an exoskeleton mechanism constructed of closed loops with the finger segments was adopted such as done in [24] [25] [26] [27] [28], to move MP and PIP joints. The mechanism was attached to middle and proximal segments of finger in

a distance of 35 and 15 mm respectively from MP and PIP joints with assumption of not moving. Fully actuated design of mechanisms for extension/flexion of index finger with two DOF and thumb with one DOF are shown in Figure 38 and Figure 39.

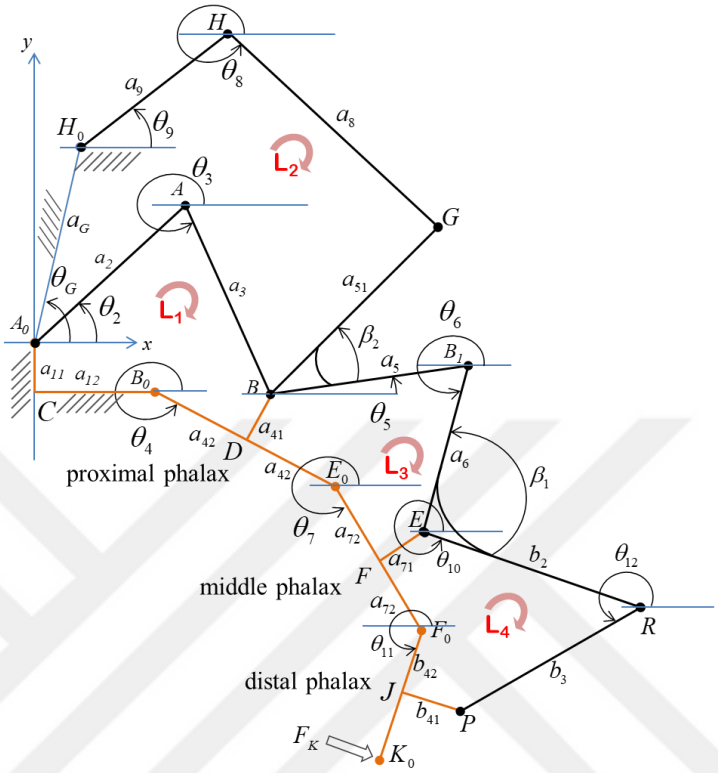

Figure 38: Fully-actuated mechanism for index finger

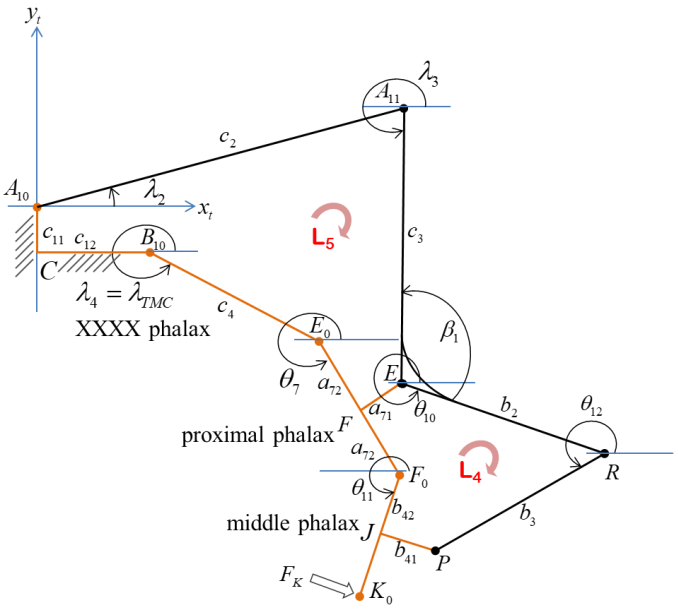

Figure 39: Fully-actuated mechanism for thumb finger

CHAPTER 6

SYNTHESIS AND OPTIMIZATIN OF MECHANISISM

Optimal mechanism synthesis is crucial for the efficient robotic control. Its main target is the generation of a trajectory from start to goal that satisfies objectives, such as minimizing the path traveling distance or time interval, lowest energy consumption and satisfying the mechanism's kinematics and dynamics. There are many works on mechanism synthesis which roughly can be divided to analytical methods and computational methods with kinematics or kinetics approaches.

In the kinematic synthesis, the objective is to calculate the mechanism dimensions required to achieve or approximate the prescribed mechanism output parameters. Calculated mechanism dimensions include link lengths, link positions, and joint coordinates. Prescribed mechanism output parameters include link positions, path points, and displacement angles. Because the calculated outputs in kinematic synthesis are basically mechanism dimensions, kinematic synthesis is also called dimensional synthesis. In contrast to kinematic analysis, where mechanism dimensions are known and the resulting mechanism output parameters are calculated in kinematic synthesis, mechanism output parameters are known and the corresponding mechanism dimensions are calculated [29].

In the synthesis process, the model is optimized considering the transmission angle of the mechanism in the coupler positions. Exact coupler positions are attained with transmission angles not more than difference of the optimum value of 90 degrees[30]. The link lengths and structure of the proposed mechanism is emerged as a result of the kinematics and kinetics-based optimization criteria.

In order to implement the control on MP and PIP joints practically, we have designed an exoskeleton mechanism [28, 31-33]. The fully-actuated 2 DOF of mechanism is designed consisting of 4 four-bar loops in a way that two actuators drive the MP and PIP directly and DIP is driven indirectly as a function of MCP and the PIP joints. In the extension/flexion plane, the index finger has 3 degrees of freedom. However, as the exoskeleton mechanism is coupled to the index finger, total system is reduced to 2 degrees of freedom. This reduction is achieved so as to decrease the number of the actuators and to simplify the mechanism.

The exoskeleton mechanism is synthesized by the multi-objective optimization concerning the transmission angles [34] and the desired kinematics of the healthy index fingers in the cost function. Figure 38 shows the general structure of the exoskeleton on the index finger. The parameters of the system are obtained by the genetic algorithm as the optimization technique. The proposed fully-actuated mechanism has 2 degrees of freedom to excite the index finger in extension/flexion plane. However, the index finger has 3 DOF in this plane. The nature of the mechanism utilizes the kinematic relation between the PIP and DIP angles [1]. Loop 4 is designed to make DIP angle trace a related function depending on MCP and PIP angles. It is seen that the pinching kinematics may reveal certain variations among people. The fixed function for DIP joint angle therefore may provide some drawbacks when mirror therapy is considered.

θ_4, $\theta_7$and θ_{11} are MCP, PIP, and the DIP joint angles of the finger respectively. Inputs to the Exo-finger are given through θ_2 andθ_9. The mechanism design requires finding the parameter vector, V, which minimizes a cost function J. The parameter vector becomes the design vector for the optimization problem. The design vector with 16 parameters to be optimized is given as below.

$V = \{a_2, a_3, a_{41}, a_5, a_{51}, a_6, a_{71}, a_8, a_9, b_2, b_3, b_{41}, a_G, \theta_G, \beta_1, \beta_2\}$

Wherea_{41}, $a_{71}$and $b_{41}$are the lengths of the rings to couple the mechanism to the phalanges. The location of actuator, i.e. the dc motor at A_0 with respect toB_0, namely the MCP joint is fixed by given the parameters a_{11}anda_{12}. The location of the second actuator at $H_0$with respect to the first one is defined by $a_G$andθ_4. They are included in the design vector as well. β_1 and $\beta_2$are the structural angles of the ternary links at joints E and B respectively. Remaining of the elements of the design vector define the link lengths of the mechanism as shown Figure 38. Finallya_{42}, $a_{72}$and $b_{42}$are the parameters that define the lengths of the phalanges which are determined as the mean values of the adult fingers [2].

The cost function, J, in the multi-objective optimization algorithm is given as below.

$$J_1 = \frac{1}{4N}\left(\sum_{i=1}^{N}\left((\gamma_{11}(i) - \frac{\pi}{2})^2 + (\gamma_{21}(i) - \frac{\pi}{2})^2 + (\gamma_{31}(i) - \frac{\pi}{2})^2 + (\gamma_{41}(i) - \frac{\pi}{2})^2\right)\right)$$

$$J_2 = \frac{1}{4N}\sum_{i=1}^{N}((\gamma_{12}(i) - \frac{\pi}{2})^2 + (\gamma_{22}(i) - \frac{\pi}{2})^2 + (\gamma_{32}(i) - \frac{\pi}{2})^2 + (\gamma_{42}(i) - \frac{\pi}{2})^2)$$

$$J_3 = \frac{1}{N}(\sum_{i=1}^{N}(\theta_{11}(i) - \theta_{11d}(i))^2)$$

$$J = \alpha_1 J_1 + \alpha_2 J_2 + \alpha_3 J_3$$

J is composed of 3 components. $J_1$and J_2 reflect the design concerns about the transmission angles which are desired to be kept close to π/2 rad. $J_3$is used to make the DIP joint, θ_{11}, track the desired function in terms of MCP and PIP joints, $\theta_4$and θ_7 respectively. N is the number of data points. In the componentJ_3, $\theta_{11d}$is the desired DIP joint angle to obtain a natural pinching kinematics?

By tuning the weighting factors (α1, α2 and α3) we can emphasize on tracking requirement or transmission angles. Increasing α1 and α2 and decreasing α3, less emphasis is given to the tracking requirement and transmission angles are much more critical. Increasing α3 and decreasing α1 and α2, less emphasis is given to the transmission angles and tracking is much more critical.

The backward transmission angles γ_{i1} for $i = 1,..,4$ are the angles(A_0AB), (H_0HG) , $(BB_1E)$and (ERP) respectively for each loop. They are critical for the feasible mechanism design and the back-drivability of the mechanism by the voluntary finger motions. Therefore, the cost function includes the squares of the deviations of the backward transmission angles from π/2. The forward transmission angles $\gamma_{i2}$for $i = 1,..,4$ are the angles(ABB_0), (HGB) , (B_1EE_0) and (RPF_0) respectively for each loop. They are critical to reach feasible mechanism designs as well. In addition, these angles are important for the drivability of the mechanism by the actuators. Therefore, the cost function includes the squares of the deviations of the forward transmission angles from π/2. This helps to minimize the required actuator torques to attain the desired kinematics. The transmission angles are defined as below.

Backward transmission angles:

$$\gamma_{11} = \theta_3 - \theta_2 - \pi, \gamma_{21} = \theta_8 - \theta_9 - \pi, \gamma_{31} = \theta_6 - \theta_5 - \pi, \gamma_{41} = \theta_{12} - \theta_{10} + \pi$$

Forward transmission angles:

$$\gamma_{12} = \theta_4 - \theta_3 - \tan^{-1}(\frac{a_{42}}{a_{41}}) + \frac{\pi}{2}, \gamma_{22} = \theta_5 - \theta_8$$

$$\gamma_{32} = \theta_7 - \theta_6 - \tan^{-1}(\frac{a_{72}}{a_{71}}) + \frac{\pi}{2}, \gamma_{42} = \theta_{11} - \theta_{12} - \tan^{-1}(\frac{b_{42}}{b_{41}}) + \frac{\pi}{2}$$

To sum up, the mechanism design procedure is finding the optimal design vector V to minimize the given objective function J.

$$V^* = \arg\min_V J(V) \; such\; that \begin{cases} c_{eq}(V) = 0 \\ LB \leq V \leq UB \\ inverse\; kinematics \end{cases}$$

Where c_{eq}refers to the nonlinear equality constraint to reach physically realizable mechanisms forcing the kinematic solutions of the joint angles to be real numbers. Considering the physical application, lower and upper bounds (LB and UB respectively) are defined for the parameters as well. This is essential to design a compact Exo-finger with reduced inertia on the human finger.

It is seen that J depends on the angular variations of the mechanism in terms of transmission angles and DIP joint angle. In order to calculate the cost function and the nonlinear equality constraint, kinematic equations and solutions are required. The inverse kinematics solutions are employed to calculate the joint angles for Loops 1, 2 and 3 due to the given proximal and middle phalanges pinching motion; namely the required θ_4 and $\theta_7$for pinching motion are given and necessary kinematic inputs in terms of θ_2 and θ_9 are calculated at each optimization step. In addition, desired θ_{11} as a function of θ_4 and θ_7 is calculated at each step as well. Using direct kinematics equations for Loop 4, $\theta_{11}$is calculated with the available link dimensions. Using these kinematic solutions values of the cost function and the nonlinear constraint equation are calculated. Optimization procedure is summarized in Figure 40.

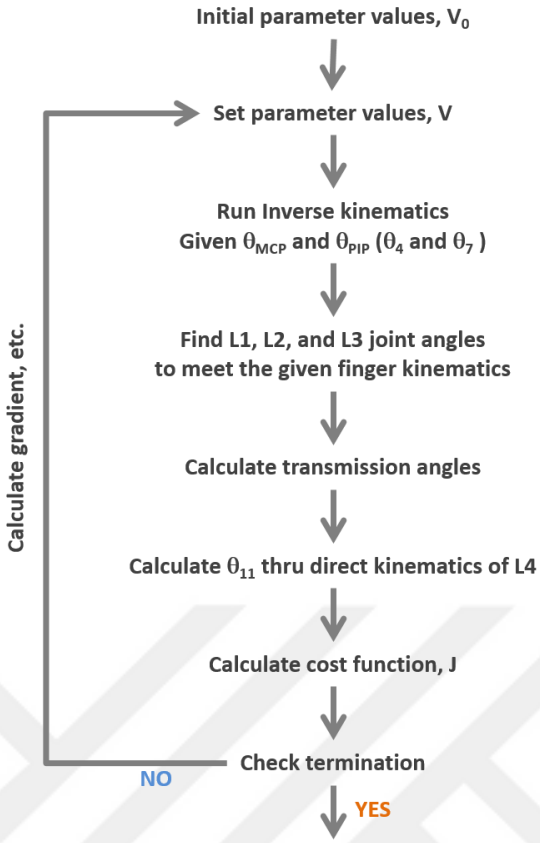

Figure 40: Optimization Process

So as to perform these calculations of concern, direct and inverse kinematic equations are generated and solved based on the following loop-closure equations as shown below.

Loop 1 (L1): $a_2e^{i\theta_2} + a_3e^{i\theta_3} = (-a_{11}i + a_{12}) + a_{42}e^{i\theta_4} + a_{41}e^{i(\theta_4+\frac{\pi}{2})}$

Loop 2 (L2): $a_Ge^{i\theta_G} + a_9e^{i\theta_9} + a_8e^{i\theta_8} = a_2e^{i\theta_2} + a_3e^{i\theta_3} + a_{51}e^{i(\theta_5+\beta_2)}$

Loop 3 (L3): $a_{41}e^{i(\theta_4+\frac{\pi}{2})} + a_5e^{i\theta_5} + a_6e^{i\theta_6} = a_{42}e^{i\theta_4} + a_{72}e^{i\theta_7} + a_{71}e^{i(\theta_7+\frac{\pi}{2})}$

Loop 4 (L4): $a_{71}e^{i(\theta_7+\frac{\pi}{2})} + b_2e^{i\theta_{10}} + b_3e^{i\theta_{12}} = a_{72}e^{i\theta_7} + b_{42}e^{i\theta_{11}} + b_{41}e^{i(\theta_{11}+\frac{\pi}{2})}$

Input and the output considerations for each loop is given in Table 6.

Table 6: Given/Calculated Joint Angels from direct and inverse kinematic equations

	Direct Kinematics		Inverse Kinematics	
	Given	Calculated	Given	Calculated
L1	θ2	θ3, θ4	θ4	θ2, θ3
L2	θ2, θ3, θ9	θ5, θ8	θ2, θ3, θ5	θ8, θ9
L3	θ4, θ5	θ6, θ7	θ4, θ7	θ5, θ6
L4	θ7, θ10	θ11, θ12	θ7, θ11	θ10, θ12

Note that $\theta_{10}$is a function of θ_6 as given below.

$\theta_{10} = \theta_6 + \pi - \beta_1$

While the kinematic characteristics of the mechanism is being considered, for a constant torque input, in a well performing mechanism the maximum torque output and the minimum bearing forces must be obtained. Transmission angle is a simple parameter in which neither the forces nor the velocities are taken into consideration but the behavior of the mechanism under the dynamic forces can be judged in the kinematic design stage.

By definition sin of transmission angle is the ratio of force component tending to move driven link to total force applied to driven link. Clearly, the optimum value of the transmission angle is 90 degrees. When the mechanism moves the transmission angle constantly changes and deviate from 90. In practice the maximum deviation of the transmission angle from 90 should be 40 or 50 degrees otherwise the mechanism will lock [34].

Genetic algorithm is used as the optimization algorithm. The problem is a multi-objective one, due to the concerns about transmission angles and the need to track a desired function forθ_{11}. More or less emphasis to the prescribed objectives is described by the selection of $\alpha_i$values. It is seen that sub costsJ_1, $J_2$and J_3 are compromising functions. Especially $J_1$and J_3which reflect the optimization of backward transmission angles and tracking the desired angle θ_{11} respectively. Due to this trade off, the optimization algorithm reveals feasible designs that satisfy each requirement to a certain extent. Therefore depending on the constraints, bounds and the weightings, various designs are obtained.

Global Optimization Toolbox of Mat-Lab and its Nonlinear Constraint Algorithm was utilized for the optimization process. "This algorithm uses the Augmented Lagrangian Genetic Algorithm (ALGA) to solve a nonlinear optimization problem with nonlinear constraints, linear constraints, and bounds, without integer constraints. In this approach, bounds and linear constraints are handled separately from nonlinear constraints. A sub-problem is formulated by combining the fitness function and nonlinear constraint function using the Lagrangian and the penalty parameters. A sequence of such optimization problems are approximately minimized using the genetic algorithm such that the linear constraints and bounds are satisfied."[35, 36]

Weighting factors α1, α2 and α3 were tuned at 0.1, 0.45 and 0.45 respectively. An initial population with 3000 individuals was considered.

As a result of optimization, all the elements of the design vector and link lengths of the mechanism defined in Figure 38 are listed below (dimensions units are centimeter and angle units are degree).

Motor positions are $X_{A0} = 0,\ Y_{A0} = 0,\ Z_{A0} = 0,\ Z_{B0} = 0,\ Z_{H0} = 0,\ X_{aG} = -3.85, Y_{aG} = 0.$

Links lengths are $a_{42} = 3.5, a_{43} = 1.5, a_{12} = 4, a_{11} = 3.2, a_2 = 5, a_3 = 4.7, a_{41} = 3,\ a_{71} = 5.5,\ a_{72} = a_{73} = 1.5,\ b_{42} = b_{43} = 1.25,\ a_5 = 5,\ a_6 = 4.5,\ a_9 = 8,\ a_8 = 9.5, a_{51} = 3.5, b_2 = 2.5\ , b_3 = 4.9, b_{41} = 3.$

Fixed angles are $Beta_1 = -95, Beta_2 = 10.$

Based on the optimization results we simulated the system to show the trade-off between forward and backward transmission angles and tracking the desired pattern for index finger. Movement of total system during pinching action for index finger is shown in Figure 41 and tracking the desired pattern for θ_{11}shown in Figure 42 and finally forward and backward transmission angles can be seen in Figure 43.

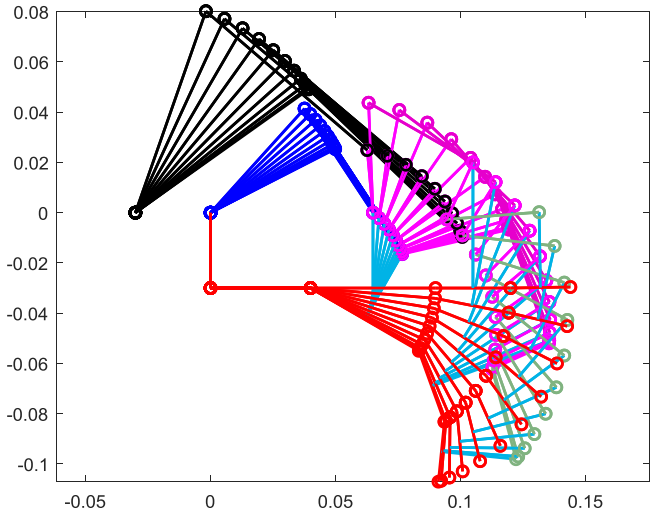

Figure 41: Movement of total system

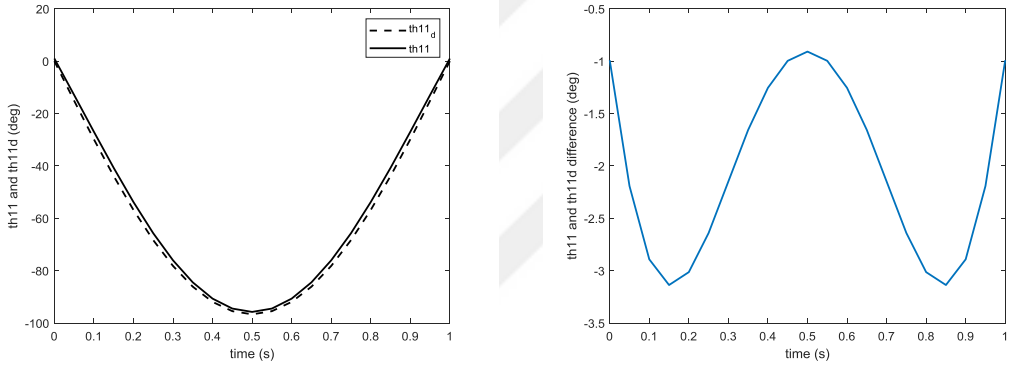

a) Pattern of $\theta_{11}$and θ_{11d}during pinching b) Diffrence between $\theta_{11}$and θ_{11d}

Figure 42: Tracking the desired pattern

It can be seen that θ_{11} tracks the desired pattern with maximum 3 degrees of error.

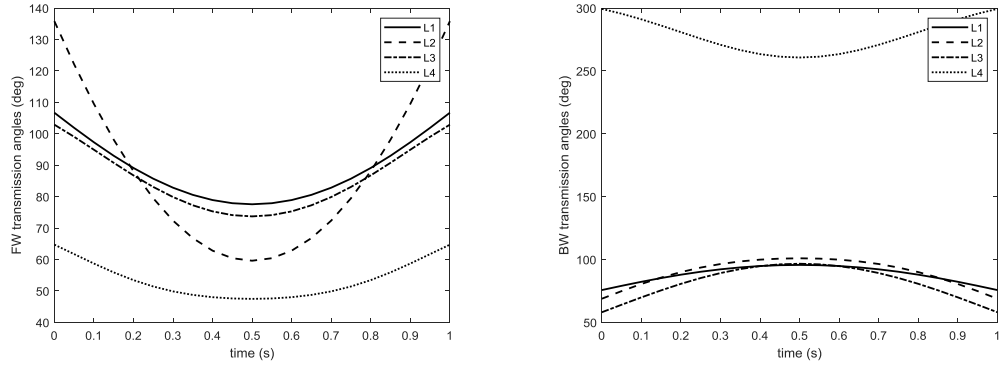

a) Forward transmission angles b) Backward transmission angles

Figure 43: Forward and backward transmission angles for loops 1-4

Figure 44 shows the deviation of transmission angles from 90 degrees, corresponding to loops 1, 2, 3 and 4 which was extracted from MatLab-Simmechanics model.

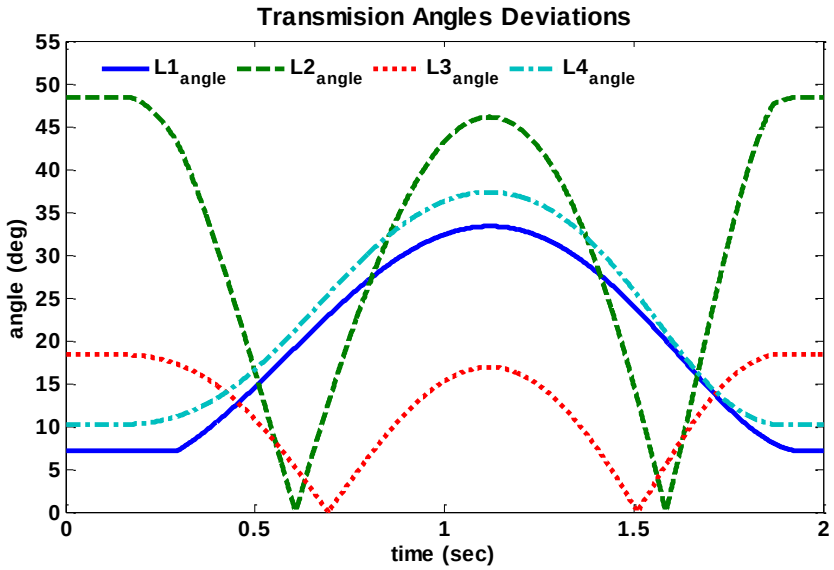

Figure 44: Deviation of transmission angles from 90 corresponding to loops 1-4

It can be seen that deviation of transmission angles are less than 50 degrees which is an acceptable value

6.1 Detail model in SOLIDWORKS

As before mentioned models in MatLab and MatLab-Simmechanics do not include the low level details for the links, connections, and the joints. In order to produce the Exo-finger system, detailed design should be performed with structural analysis. So we designed the complete Exo-finger system in Solidworks and exported it to MatLab-Simmechanics for further analysis. The solid model of the index finger and thumb finger in Solidworks for extension/flexion movements are shown in Figure 45 .

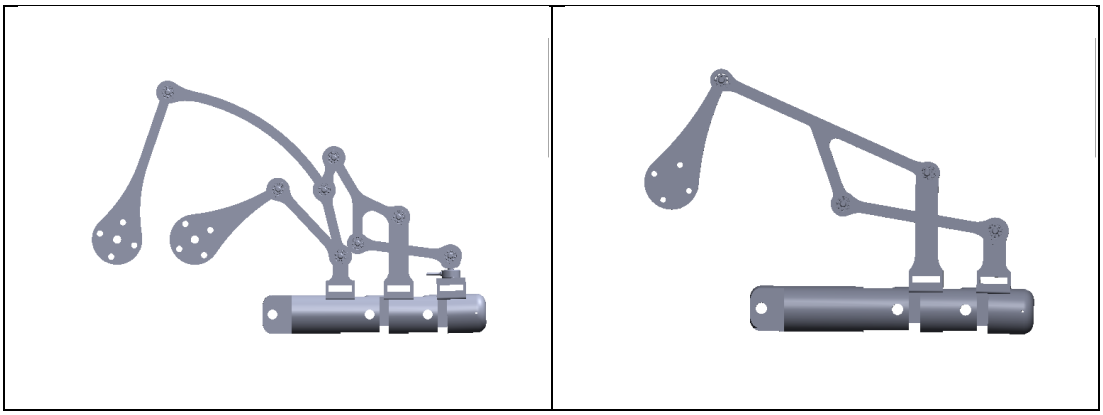

Figure 45: solid model of the index finger and thumb finger in Solid-works

Total Exo-pinch system with 4 DOF shown in Figure 46 were designed in Solid-works. The mechanism has 2 DOF for extension/flexion of index finger and 1 DOF for extension/flexion of thumb finger another DOF for thumb finger is used for abduction motion.

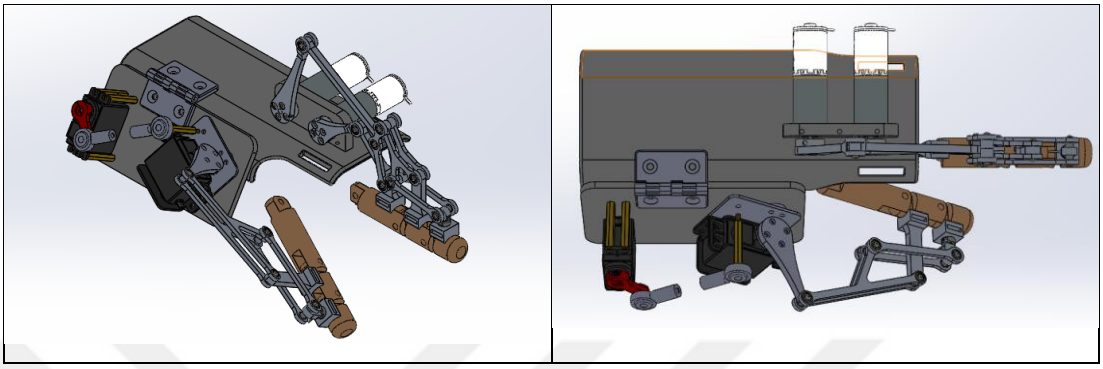

Figure 46: Total Exo-pinch mechanism in Solid-works

6.2 Fabrication

In regard to all design process, explained before, we fabricated two prototype for Exo-pinch mechanism.

The first prototype shown in Figure 47, has 3 DOFs, one for extension/flexion of thumb and two for extension/flexion of index finger. All abduction and adduction motions are passive. The mechanism links were manufactured by 3-D printer from ABS (Acrylonitrile butadiene styrene) which is a common engineering thermoplastic polymer. The actuators are HSR-5980SG HMI High Torque, Steel Gear Robot Servo motors which are controlled by Pololu Mini Maestro servo controller in Simulink environment.

This Exo-pinch system was tested on healthy people and patients in many instances. The advantages of this prototype is that, it is light and easy to control. But only position control can be applied on this system. Anyway the results were satisfactory, because we did many experiments on patients with this system.

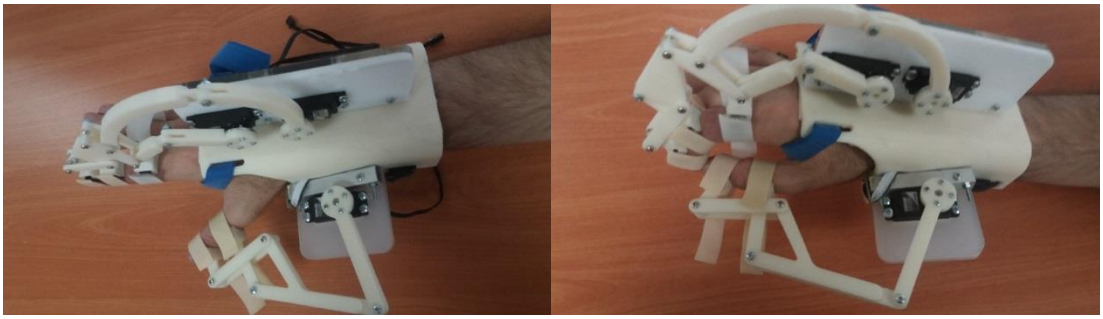

Figure 47: Designed and manufactured mechanism of index finger (first prototype)

The final prototype shown in Figure 48, has 4 DOFs, one for extension/flexion of thumb and two for extension/flexion of index finger another DOF is used to control abduction of thumb finger. Other abduction and adduction motions are passive. The mechanism links were manufactured from high strength Aluminium metal, which is the lightest common engineering metal. The actuators are two 24 volt DC motors (with 3 Nm stall torques) and two HSR-5980SG HMI High Torque, Steel Gear Robot Servo motors which are controlled by Humusoft Data Acquisition and Control Board (MF624) in Simulink Desktop Real-Time environment.

This Exo-pinch system was tested only on healthy people many times. The advantages of this prototype is that, not only position control can be applied, but also torque control can be done on this system for extension/flexion of index finger. At the same time we can observe the motor torques and estimate the torques applied on the index finger joints. Another advantage of this prototype is that the abduction motion of thumb finger can be controlled, so the pinching motion will be more realistic. The only disadvantage of this system in compared with previous one is that it is heavier with respect to previous prototype. The results were again acceptable, since we did many tests on healthy people with this system.

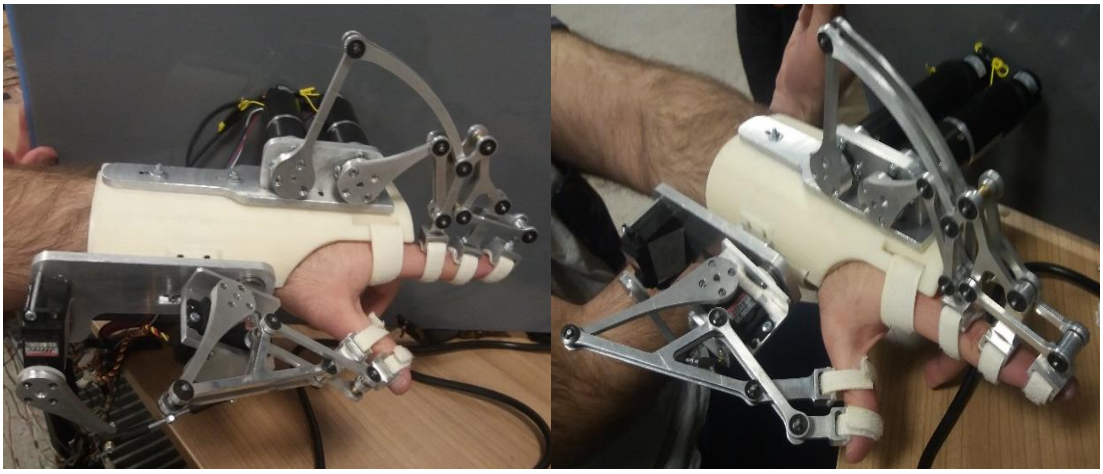

Figure 48: Designed and manufactured mechanism of index finger (final prototype)

Based on the fully actuated design of mechanism for index finger and thumb finger shown in Figure 38 and Figure 39, index finger and thumb exoskeletons and their corresponding links and joints are shown in Figure 49 and Figure 50.

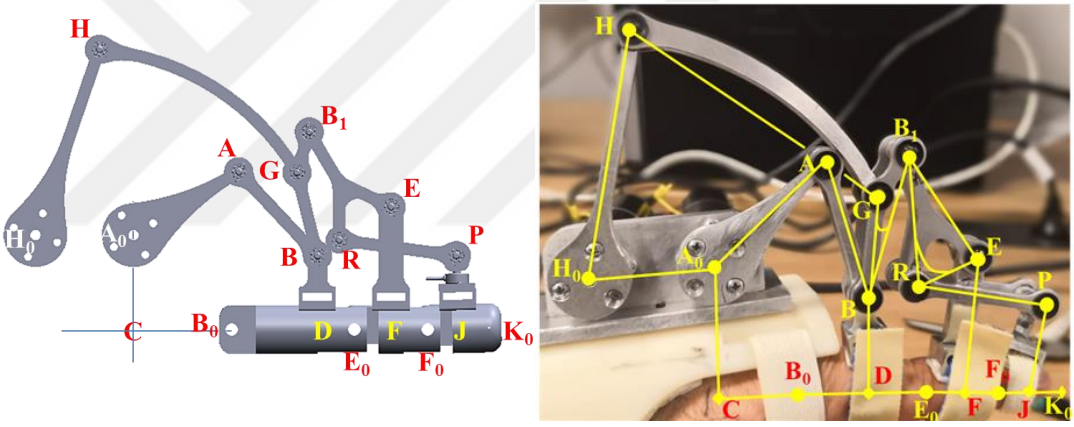

Figure 49: Index finger and corresponding links and joints

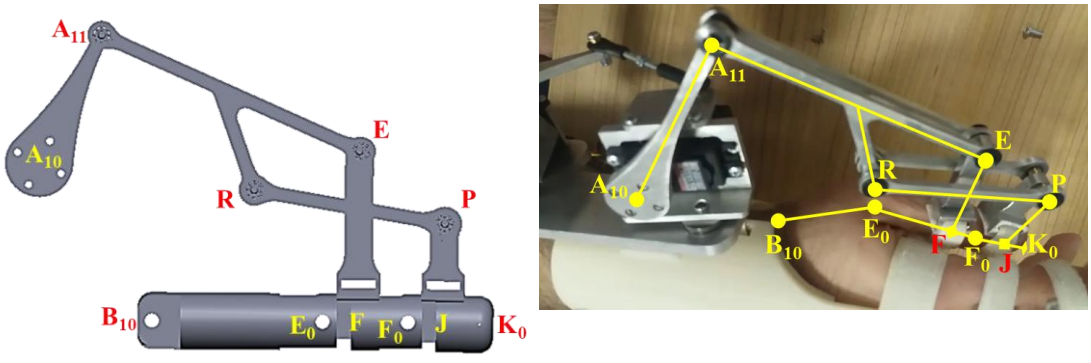

Figure 50: Thumb finger and corresponding links and joints

6.3 Model in SIMMECHANICS

Multi-body dynamical model for the index finger is built in MatLab-Simmechanics as shown in Figure 51. Required motor torques to obtain the desired kinematics are calculated by using the inverse kinetics model in Simmechanics firstly.

The actuators, M_1andM_2, are placed at $A_0$and H_0respectively. The designed model is exported to MatLab-Simmechanics from Solidworks for the kinematic and kinetic analysis was done.

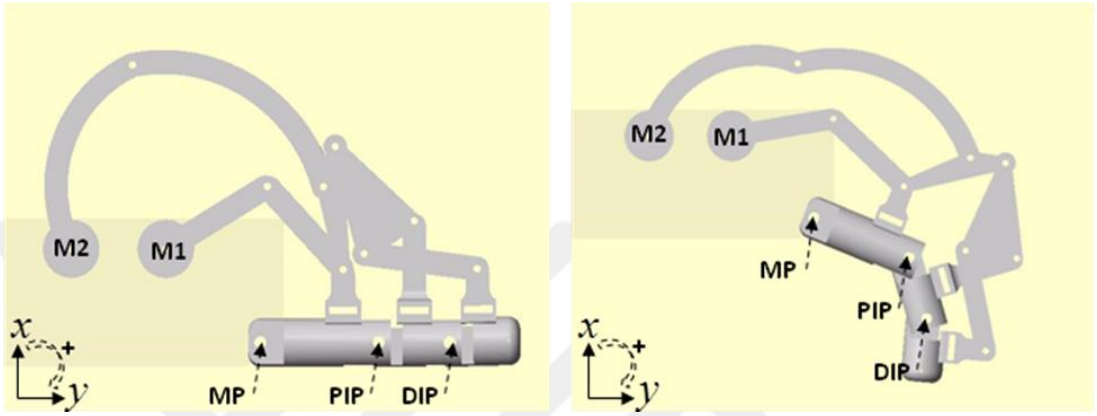

Figure 51: Index finger mechanism in MatLab-Simmechanics

6.4 Index finger passive dynamic torques

The simplified model for the human index finger is illustrated in Figure 52. It consists of three joints and four segments in the extension-flexion plane [21].

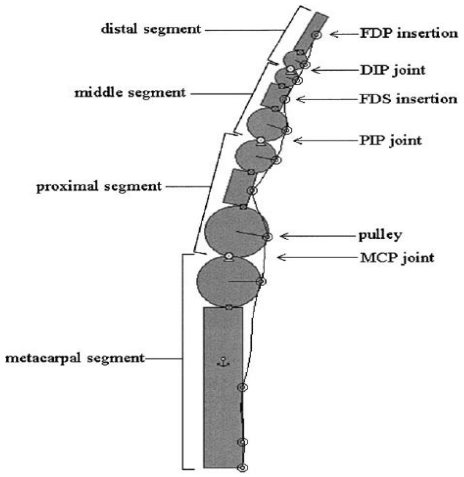

Figure 52: Model of human index finger [21]

The human finger has passive joint torques as resistances to motion [21]. Typical model for a healthy subject is given as below. This model is introduced for each joint in our kinetic model, as well.

$\tau_j = \tau_j^s - B_j\dot{\theta}_j - K_j\Delta\theta_j$

Where τ_j is the passive joint torque, τ^s a function of $(\theta_j - \theta_{j+1})$, is the static passive torque, and B and K (a function of θ_j) are the damping and dynamic stiffness coefficients for joint j. The static torque was computed for the difference in joint angle between the each link and the previous joint extension. The value of $\Delta\theta$ was results of the subtraction of current joint angle from 5 milliseconds obtained from the model simulation using the MatLab-Simmechanics.

The physiological static passive joint torque is demonstrated in Table 7, and the stiffness and damping at each joint are demonstrated in Table 8 as presented in [21].

Table 7: Static passive torque at each joint

Joint	$\tau^s(N.m)$
DIP	$-0.103\theta^3 + 0.102\theta^2 - 0.052\theta - 0.019$
PIP	$0.056\theta^3 + 0.016\theta^2 - 0.132\theta + 0.015$
MP	$-0.071\theta^3 + 0.14\theta^2 - 0.154\theta + 0.0129$

Table 8: Stiffness and damping at each joint

Joint	$K(N.m/rad)$	$B \times 10^2(N.m.s/rad)$
DIP	$0.38\theta^2 - 0.09\theta + 0.13$	0.81
PIP	$1.06\theta^2 - 0.76\theta + 0.$	1.05
MP	$1.02\theta^2 - 0.54\theta + 0.45$	1.42

The order of derivative in the above equation is a positive integer and equals to 1. However, if it is fractional, the passive torque equation converts to the equation 2, where $\frac{d^\alpha}{dt^\alpha}$ is a fractional derivative with order α.

$\tau_j = \tau_j^s - B_j\frac{d^\alpha\theta_j}{dt^\alpha} - K_j\Delta\theta_j$

6.5 Controller design

In order to control the finger exoskeleton in the extension-flexion plane, two control strategies; namely the PID and the Feedback Error Learning (FEL) are used. The PID type of control architecture is given as below in Figure 53. The mathematical models for the PID controllers are given as below equations,

Where $e_1 = R_{\theta 2} - \theta_2$ and $e_2 = R_{\theta 9} - \theta_9$.

$$T_2 = K_{P1}e_1 + K_{D1}\dot{e_1} + K_{I1}\int_0^t e_1(\tau)d\tau$$

$$T_9 = K_{P2}e_2 + K_{D2}\dot{e_2} + K_{I2}\int_0^t e_2(\tau)d\tau$$

T_2 and T_9 are the torque inputs to the exoskeleton system that are applied by the motors M1 and M2 respectively. $R_{\theta 2}$ and $R_{\theta 9}$ are the reference inputs for the angular positions of the links coupled to Motor 1 and Motor 2. These references are calculated by using the inverse kinematics of the mechanism from the desired finger posture. In the simulations and the controller design, the motor drivers and motors are assumed to be ideal.

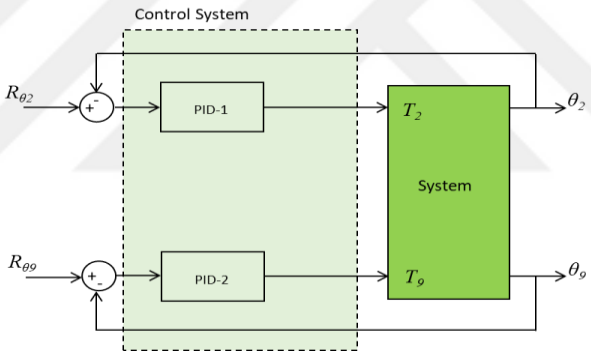

Figure 53: Architecture of PID controller

The feedback error learning (FEL) architecture in Figure 54 is an adaptive control algorithm [37, 38] . The adaptive type of controller is employed to handle the uncertainty due to the passive torques and due to the varying pinching forces during therapy that cause variable loadings on the actuators. The errors between the references and the actual angles, namely θ_2 and θ_9, of the driving links are used for online training of the multi-layer perception (MLP) type of neural network with one hidden layer[37, 38] .

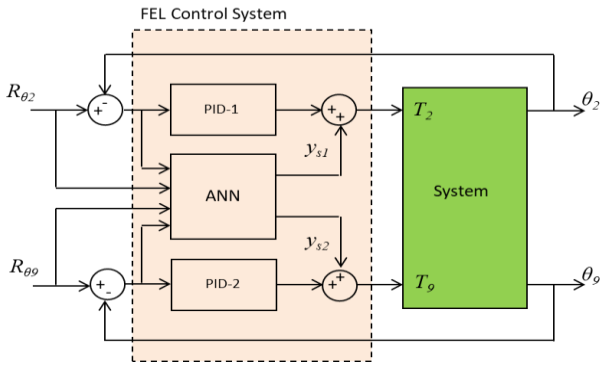

Figure 54: Architecture of FEL controller

The sigmoid activation functions are used in the ANN [39-42]. In addition to the error terms, the references are processed in the ANN, as well. The output of the network contributes as the adaptive term.

The number of the neurons in the hidden layer $N_{\mathrm{h}}$is equal to 8. Where $X_{(t)}$ represents all the "states" of the network, namely the weights and all the parameters that are calculated during the learning process. $X_{(t)}$ is updated according to an extended gradient rule as shown in equation 13. y_{s1} And y_{s2} are the outputs of the ANN and they are the adaptive parts of the control inputs. $\eta = 3.8 \times 10^{-4}$ Is the learning rate, $\frac{dys}{dX}$ is the Jacobean matrix, $T = 2 \times 10^{-4}$ is the sampling period, and $Z_{(t)}$ represents an additional contribution from a filtered error represents in equation 14. The filter decay rate, $\alpha = 0.02$ is called as the momentum term [39].

$$X_{(t+T)} = X_{(t)} + \eta \cdot \left(\frac{dys}{dX}\right) \cdot e_{(t)} + Z_{(t)}$$

$$D_{(t+T)} = \alpha \cdot D_{(t)} - \eta \cdot \left(\frac{dys}{dX}\right) \cdot e_{(t)}$$

$$Z_{(t)} = \alpha \cdot D_{(t)}$$

The model of the complete system including the controllers (PID and FEL), plant, and the passive torques in Simulink is illustrated in the Figure 55.

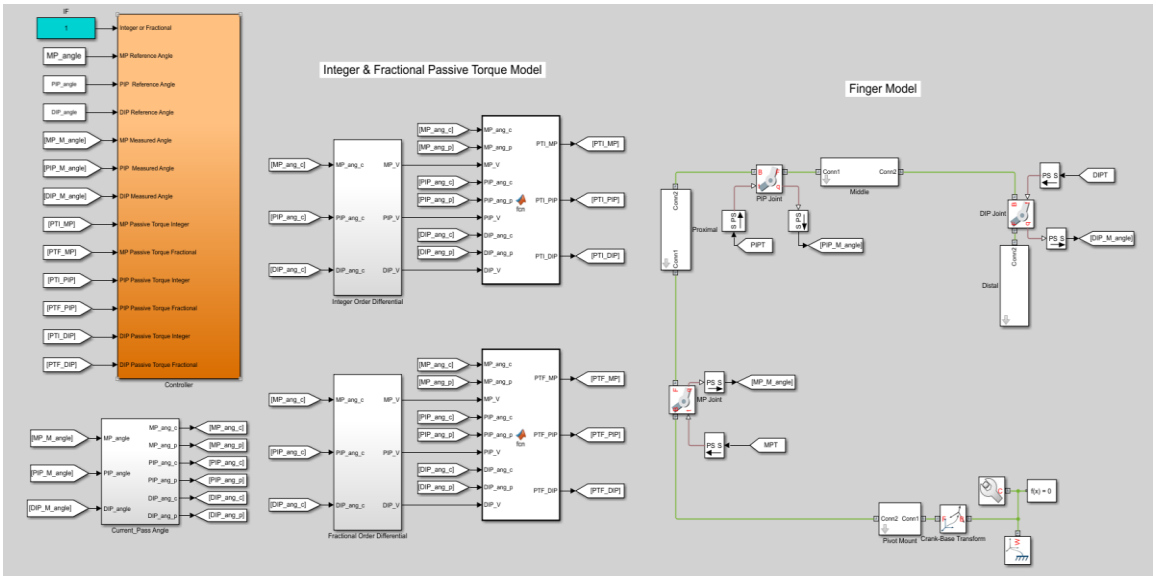

Figure 55: Block diagram of whole the system

Firstly, the reference inputs for actuators to maintain the desired pinching posture shown in Figure 56, are derived by using the inverse kinematics as given in Figure 58. Later their corresponding velocities as seen in Figure 57 and Figure 59 are derived. Then the PID controllers are tuned for the nonlinear model by using the tuning tool in the Simulink PID block.

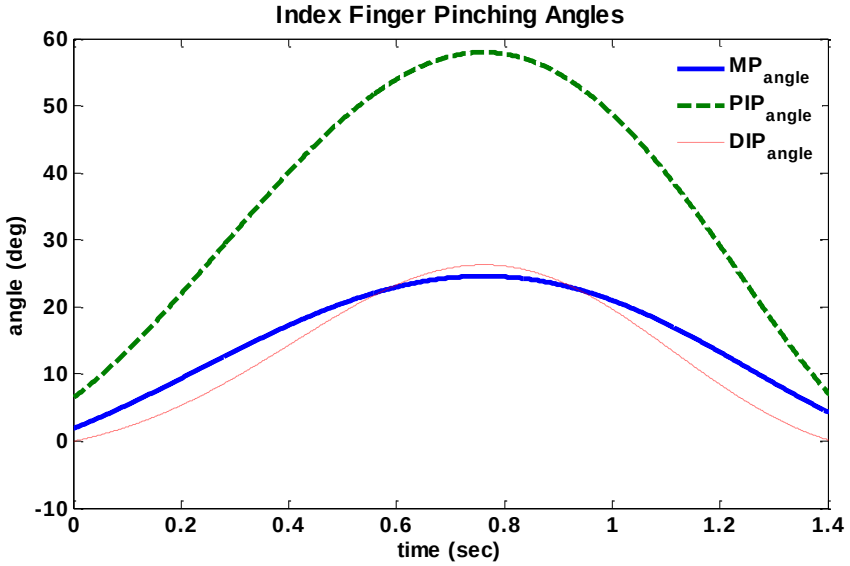

Figure 56: Index finger angles during pinching action

During the simulations of flexion index finger joint angle were as DIP 0-26.37, PIP 6.52-57.96, and MCP 1.9-24.58.

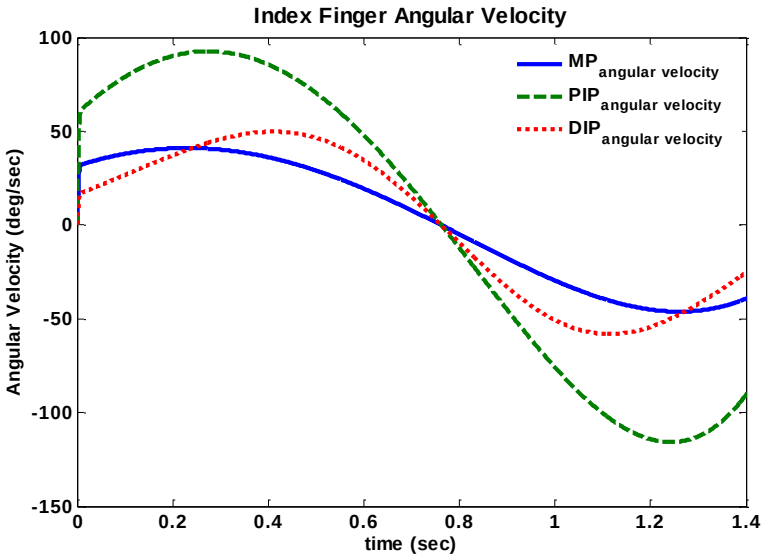

Figure 57: Index finger angular velocities during pinching action

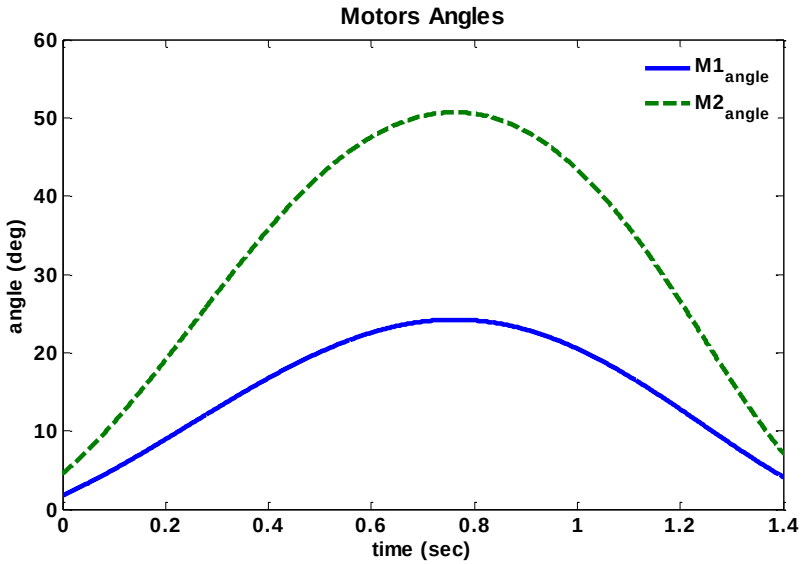

Figure 58: Motors angles during pinching action (inverse kinematics)

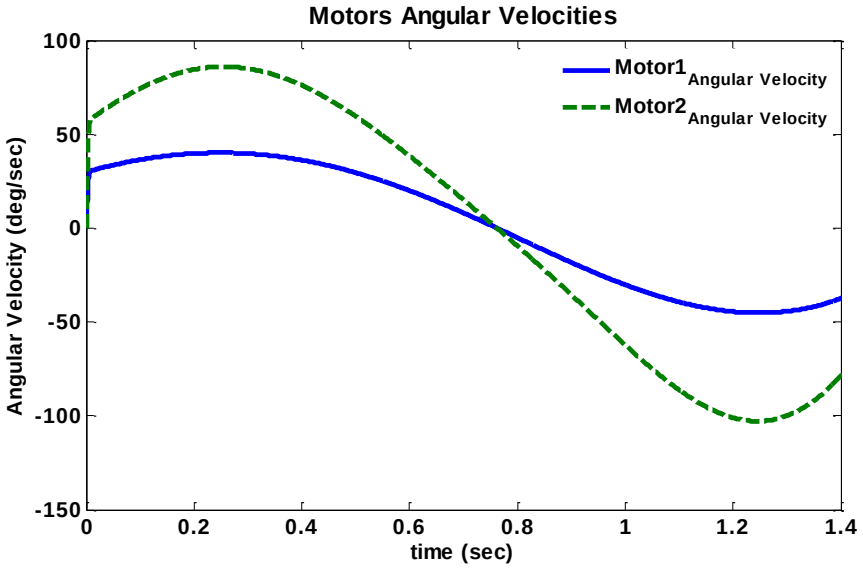

Figure 59: Motors angular velocities during pinching action (inverse kinematics)

Maximum angular velocity needed for actuators is 100.82 degree per seconds.

Dynamic passive torques of index finger joints for healthy people was derived from equations of Table 7 and Table 8. The torques shown in Figure 60, were applied on index finger joints in MatLab-Simmechanics model to extract the desired motor torques and controller output for motor torques to move the healthy peoples index finger.

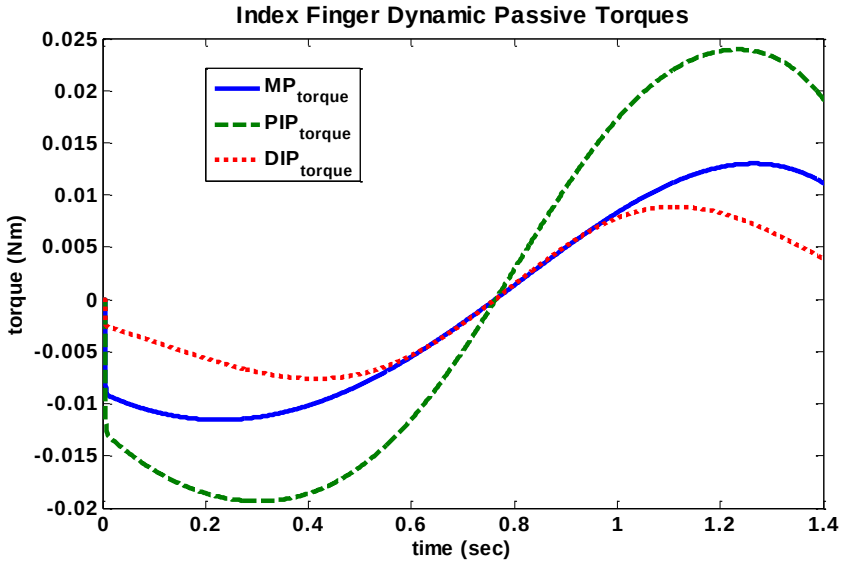

Figure 60: Dynamic passive torques of index finger joints (healthy people)

Motor desired torques extracted from inverse kinetics and controller output for motor torques to compensate passive torques on healthy fingers are shown in Figure 61 and Figure 62.

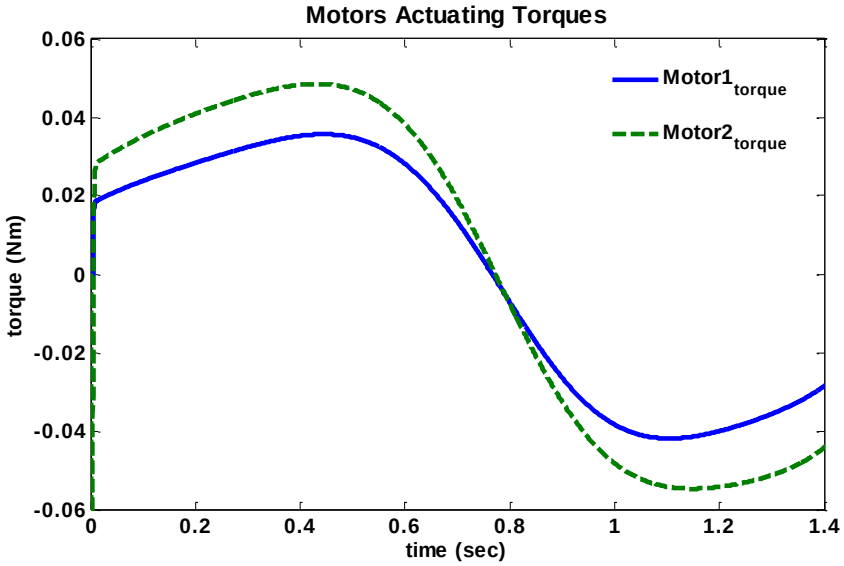

Figure 61: Motor torques for passive torques on healthy fingers (inverse kinetics)

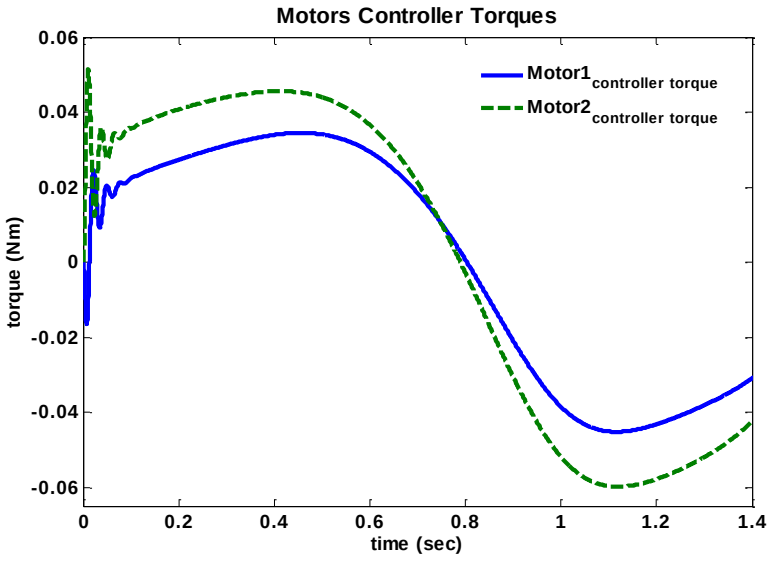

Figure 62: Controller output for motor torques (direct kinetics)

It can be seen that the motor torques needed for moving the healthy hands are not too much (less than 0.1 Nm).

But patients has spasticity in their hands and their finger can not move freely during rehabilitation. In order to select the motors, the maximum acceptable torques (MP 2.93, PIP 2.87 and DIP 1.97 Nm) on patient fingers, derived from Table 5, were used to determine the Exo-finger desired motor torques. These desired torques calculated by inverse kinetics are shown in Figure 63.

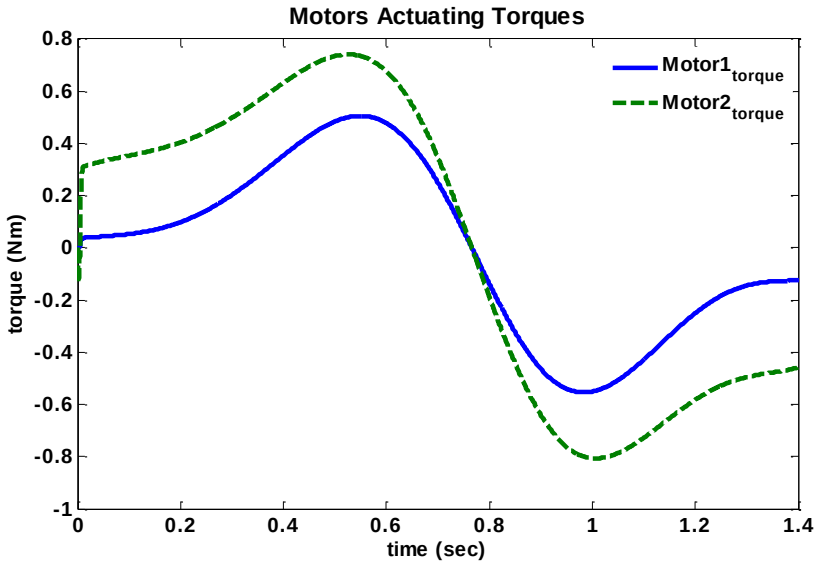

Figure 63: Motor torques for maximum acceptable torques

Motor needed torques for maximum acceptable torques on fingers helps us to select our motors. In other words our motors must generate at least 1 Nm continuous torques. For testing the designed controllers, an external force was considered on fingertip of index finger and the system was simulated and compared with and without this external force.

Motor position errors with passive torques on healthy without external force on fingertip is shown in the Figure 64.

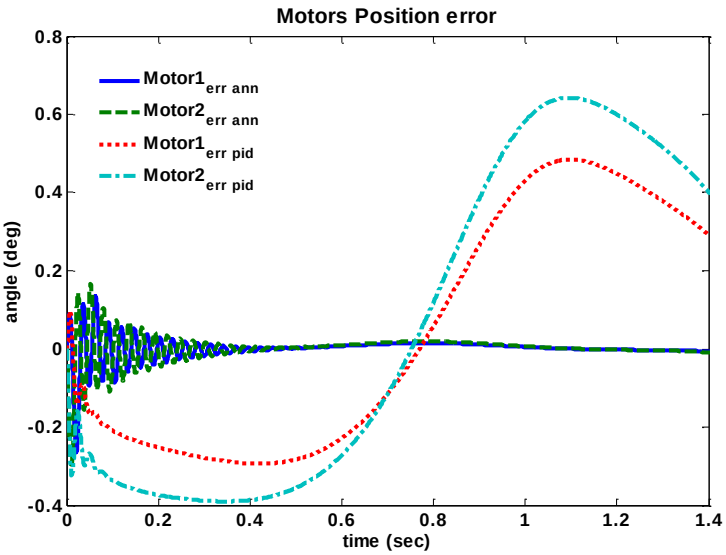

Figure 64: Maximum error comparison with PID controller and ANN controller without external force on fingertip.

Maximum error with PID controller is 0.8 degrees but with ANN controller is about 0.3 degrees

Motor position errors with passive torques on healthy fingers with 2.5N spring type external force on fingertip is shown in Figure 65.

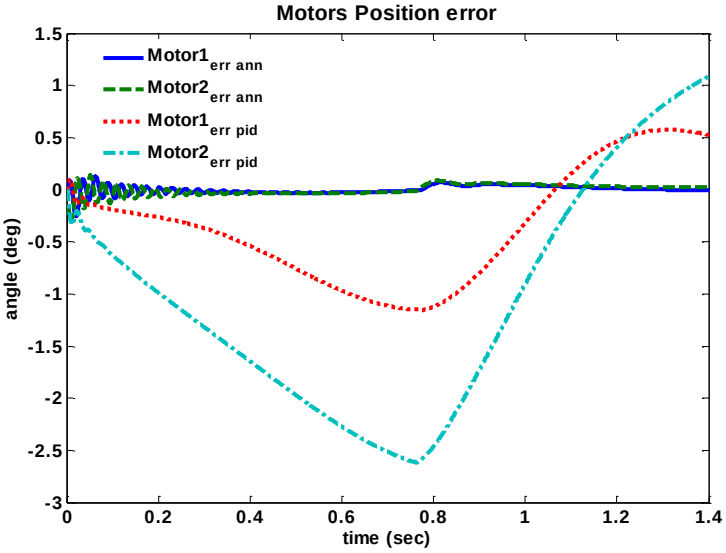

Figure 65: Maximum error comparison with PID controller and ANN controller with 2.5 N external force

Maximum error with PID controller has increased to 2.61 degrees but with ANN controller is remained at 0.3 degrees.

Motor position errors with passive torques on healthy fingers with 5N spring type external force on fingertip is shown in Figure 66.

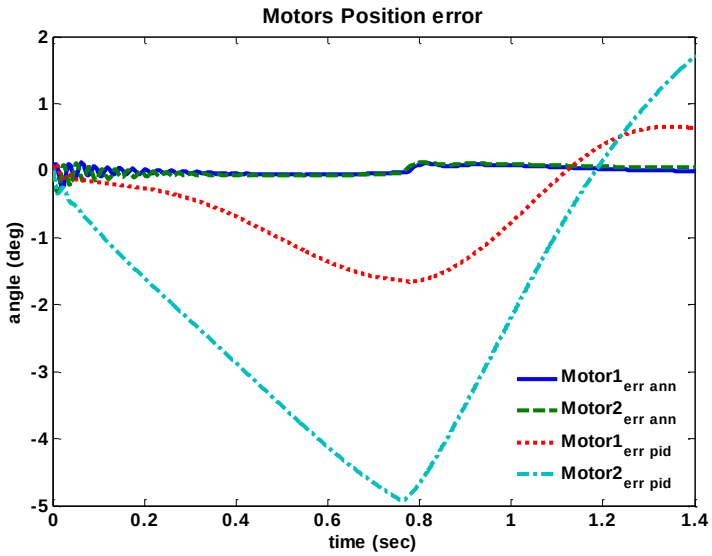

Figure 66: Maximum error comparison with PID controller and ANN controller with 5 N external force

Maximum error with PID controller has increased to 4.9 degrees but with ANN controller is remained at 0.3 degrees

Motor position errors with passive torques on healthy fingers with 10N spring type external force on fingertip external force on fingertip is shown in Figure 67.

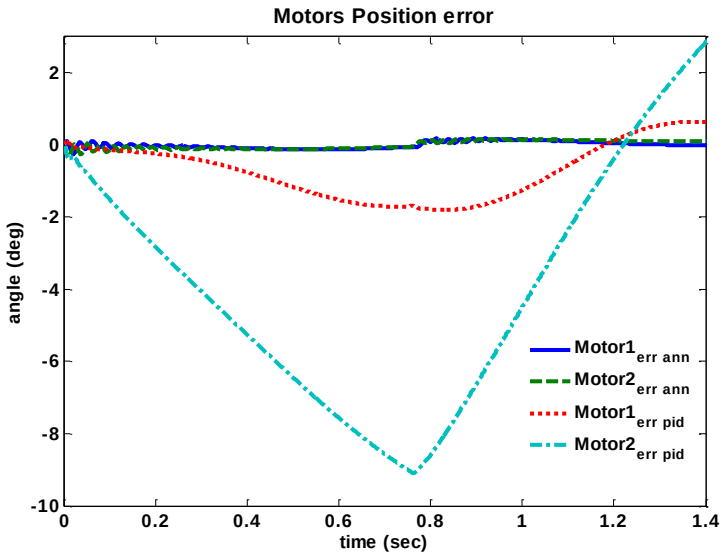

Figure 67: Maximum error comparison with PID controller and ANN controller with 10 N external force

Maximum error with PID controller has increased to 9.1 degrees but with ANN controller is remained at 0.3 degrees.

As can be seen the position error increases by increasing external force with PID controller but with ANN controller is remained constant. So ANN controller can compensate the external error successfully.

CHAPTER 7

FRACTONAL CACULUS

The order of differ-integrals in the ordinary equations is integer numbers. However, what would happen if it is fractional? Fractional calculus is the generalization of integration and differentiation that uses non-integer order operator ${}_aD_t^\alpha$ [43, 44]. There exist various definitions of the fractional differ-integral. One of the commonly used definitions is the Riemann-Lowville differ-integral, given as below [45];

$${}_aD_t^\alpha f_{(t)} = \frac{1}{\Gamma(m-\alpha)}\left(\frac{d}{dt}\right)^m \int_a^t \frac{f_{(\tau)}}{(t-\tau)^{\alpha-m+1}}\, d\tau$$

For $m-1 < \alpha < m, m \in N$, where $\Gamma(\cdot)$ is Euler's gamma function. The Grünwald-Letnikov definition is;

$${}_aD_t^\alpha f_{(t)} = \lim_{h\to 0} \frac{1}{h^\alpha} \sum_{j=0}^{\left[\frac{t-a}{h}\right]} (-1)^j \binom{\alpha}{j} f_{(t-jh)}$$

The Laplace transform of the αth derivative with $\alpha \in \Re^+$of $x_{(t)}$ relaxed at $t = 0$ is given by;

$$\left\{D^\alpha x_{(t)}\right\} = s^\alpha X_{(s)} \quad (5)$$

The below equation , presents the fractional order transfer function which is the mathematical model of the system governed by a fractional order differential equation.

$$G_{(s)} = \frac{b_m s^{\beta m} + b_{m-1} s^{\beta m-1} + \cdots + b_0 s^{\beta 0}}{a_n s^{\alpha m} + a_{n-1} s^{\alpha m-1} + \cdots + a_0 s^{\alpha m0}}$$

Where $\alpha_k, \beta_k = kq$, $k \in N$, $q \in \Re^+$, $0 < q < 1$, which q is the base order. As an example, the transfer function of a fractional derivative of order α is $G_{(s)} = s^\alpha$. The fractional-order linear time-invariant system can also be represented by a state-space model in [46];

$$D^q x_{(t)} = Ax_{(t)} + Bu_{(t)}$$

$$y_{(t)} = Cx_{(t)} + Du_{(t)}$$

The numerical methods are available for the fractional calculus, as well. The time domain and frequency methods in the form of IIR (Infinite Impulse Response) and FIR (Infinite Impulse Response) approximations are given in [46].

In this study, the time-domain response of the fractional order model is obtained using a revised Grünwald-Letnikov definition. The closed-form numerical solution to the fractional order differential equation is obtained in [44]as below equation, where h is the step-size in computation and $\omega_j^{(\alpha)}$ can be computed recursively as presented below.

$$y_t = \frac{1}{\sum_{i=0}^{n} \frac{a_i}{h^{\alpha_i}}} \left[u_t - \sum_{i=0}^{n} \frac{a_i}{h^{\alpha_i}} \sum_{j=1}^{\frac{t-a}{h}} \omega_j^{(\alpha_j)} y_{t-jh} \right]$$

$$\omega_j^{(\alpha)} = \left(1 - \frac{\alpha+1}{j}\right) \omega_{j-1}^{(\alpha)} \qquad j = 1,2, \ldots$$

$$\omega_0^{(\alpha)} = 1$$

The Ousta-loup filter gives an approximation of the fractional operators [47] in a specified frequency range (ω_b, ω_h) and of order N. Oustaloup's recursive filter for s^γ for $0 < \gamma < 1$ is given below, where $K = \omega_h^\gamma$. A refined Oustaloup filter has been proposed in [48].

$$G_f(s) = K \prod_{k=-N}^{N} \frac{s + \omega_k'}{s + \omega_k}$$

$$\omega_k' = \omega_b \left(\frac{\omega_h}{\omega_b}\right)^{\frac{k+N+\frac{1}{2}(1-\gamma)}{2N+1}} \quad , \quad \omega_k = \omega_b \left(\frac{\omega_h}{\omega_b}\right)^{\frac{k+N+\frac{1}{2}(1+\gamma)}{2N+1}}$$

$$s^\alpha = \left(\frac{d\omega_h}{b}\right)^\alpha \left(\frac{ds^2 + b\omega_h s}{d(1-\alpha)s^2 + b\omega_h s + d\alpha}\right) G_p$$

$$G_p = \prod_{k=-N}^{N} \frac{s + \omega_k'}{s + \omega_k}$$

$$\omega_k' = \left(\frac{b\omega_b}{d}\right)^{\frac{\alpha-2k}{2N+1}} \quad , \quad \omega_k = \left(\frac{b\omega_h}{d}\right)^{\frac{\alpha+2k}{2N+1}}$$

Fractional-order systems are converted to Ousta-loup objects by approximating fractional orders $\alpha \geq 1$ by $s^\alpha = s^n s^\gamma$, where n denotes the integer part of α and s^γ is obtained by the Oustaloup approximation, as presented in the mentioned references [43-48].

Since the actual order of the passive torques due to spasticity is not known, during the tuning process, various fractional orders for passive torques are utilized. The aim is to maintain a satisfactory performance of the PID controller in a certain range of the fractional order. Figure 68 reveal the passive joint torques with different orders for MP, PIP and DIP joints during PID controlled pinching action. The order was defined

in the interval [0.5-1.08]. The PID controllers alone could not maintain the stability beyond this interval.

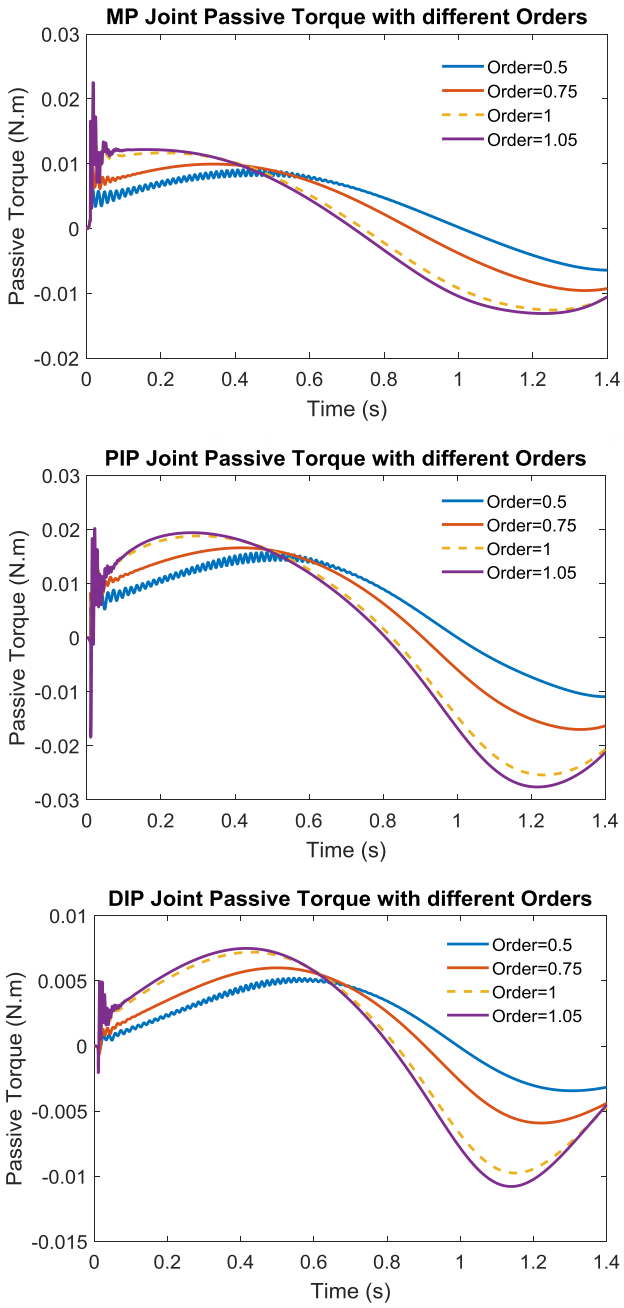

Figure 68: Passive torques with different orders for MP, PIP and DIP joints

The passive torques at MP, PIP and DIP joints in the case of using FEL controllers are demonstrated in Figure 69 as well.

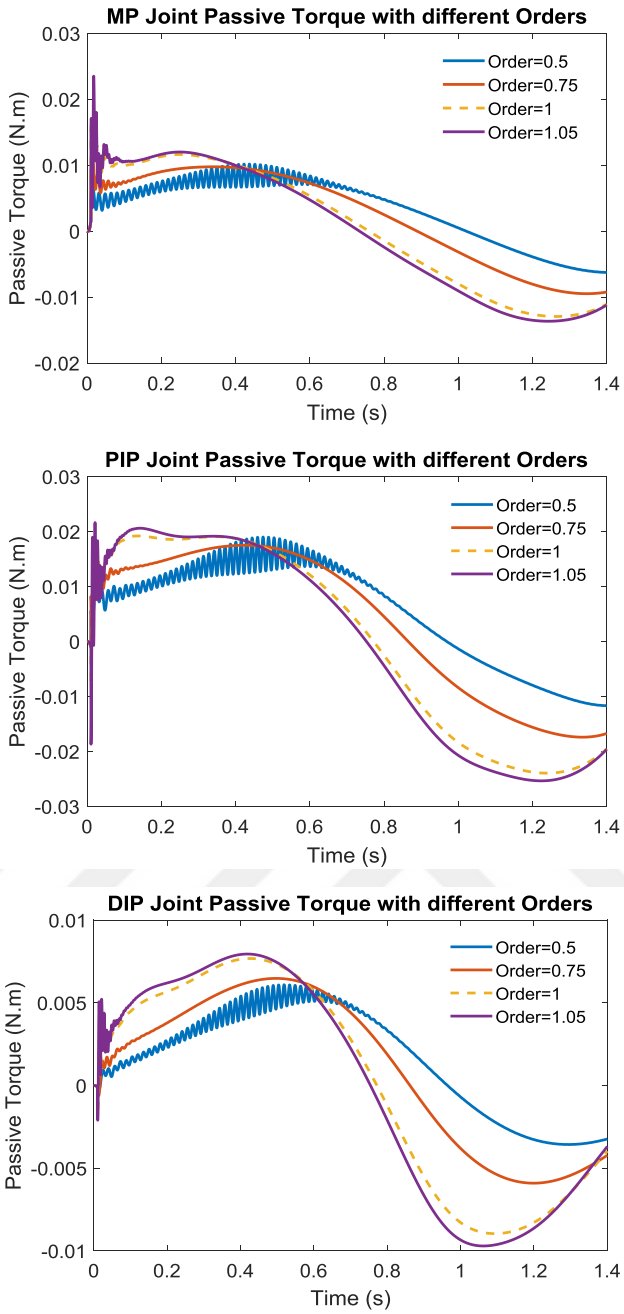

Figure 69: Passive torques with different orders (FEL applied) for MP, PIP and DIP joints

The comparison of the PID and FEL type of controllers is done based on the performances described by the following mathematical measures. The integral square error (ISE), integral absolute error (IAE), integral of time weighted absolute error (ITAE), and the root mean square error (RMSE) values were calculated and evaluated.

These measures are evaluated by usinge_i, $i = 1,2$. The equations of these error measures are given as below.

$ISE = \int e_i^2 \, dt$

$IAE = \int |e_i| \, dt$

$ITAE = \int t.|e_i| \, dt$

$RMSE = \int \frac{e_i^2}{n} dt$

An additional measure is used to evaluate the utilized control energy in terms of root mean square of the motor torque T_i , $i = 2,9$;

$RMST = \int \frac{T_i^2}{n} dt$

7.1 Simulation and Results

Firstly, the performance of both the PID and FEL controllers are compared for the integer order passive torques. The error signals of two motors are demonstrated in Figure 70. As it can be clearly seen, the FEL controller performs superior. In other words it can track the reference signal more accurately.

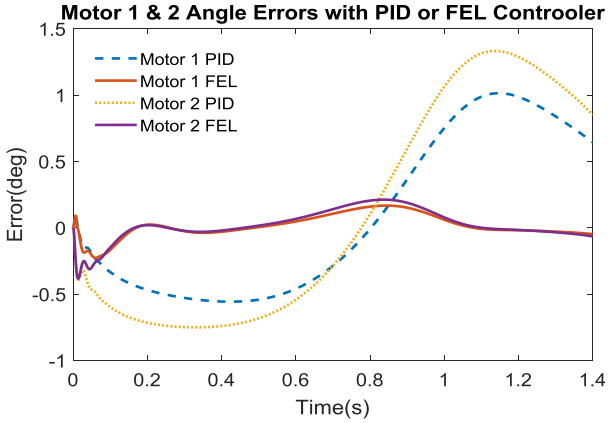

Figure 70: Error signals of two motors using by PID and FEL controllers

Secondly, the performance of the PID and FEL controllers for different sets of fractional order are investigated. The error signals in the simulations with the use of different orders of passive torques; 0.5, 0.6, 0.75, 0.9 and 1.05 respectively are presented in Figure 71.

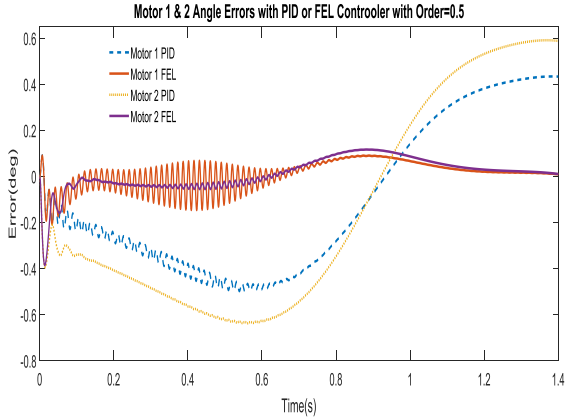
Motor 1 & 2 Angle Errors with PID or FEL Controoler with Order=0.5
Motor 1 PID
Motor 1 FEL
Motor 2 PID
Motor 2 FEL
Error(deg)
Time(s)

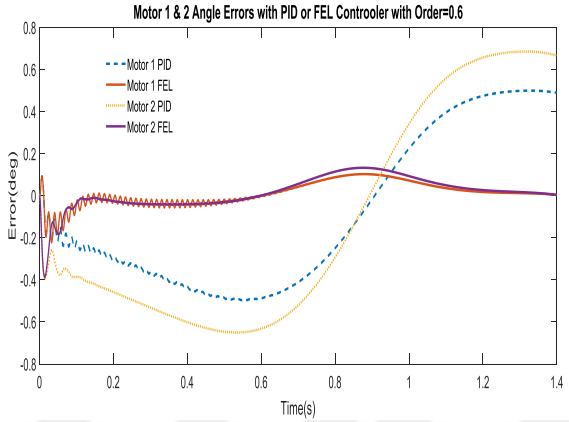
Motor 1 & 2 Angle Errors with PID or FEL Controoler with Order=0.6
Motor 1 PID
Motor 1 FEL
Motor 2 PID
Motor 2 FEL
Error(deg)
Time(s)

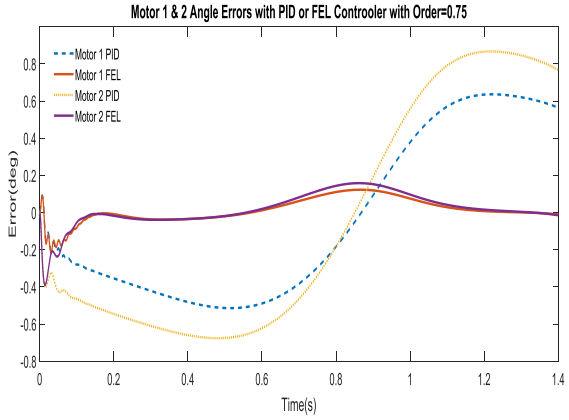
Motor 1 & 2 Angle Errors with PID or FEL Controoler with Order=0.75
Motor 1 PID
Motor 1 FEL
Motor 2 PID
Motor 2 FEL
Error(deg)
Time(s)

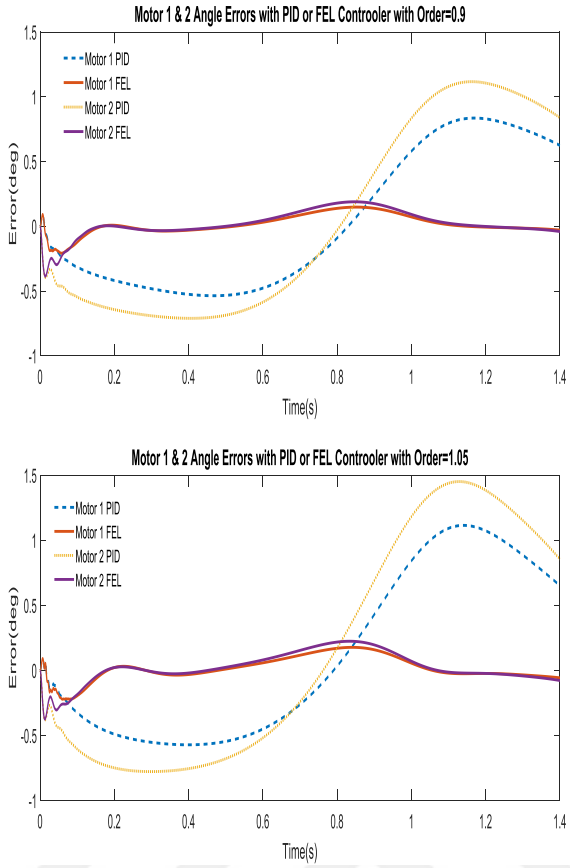

Figure 71: Error signals of two motors using by PID and FEL controllers with fractional orders; 0.5, 0.6, 0.75, 0.9 and 1.05

In order to compare the behavior of the controllers in the simulations with different fractional orders, the above mentioned error measures for the motors are derived and summarized in the Table 9 and Table 10. These tables reveal that -in all measures- FEL type control system has a superior performance when compared with that of the PID control system. The measures of the control energy, RMST, in the simulations with different fractional orders for Motor 1 and Motor 2 are presented in Figure 72. These figures show that FEL type control system consumes more control energy than that of the PID type control system.

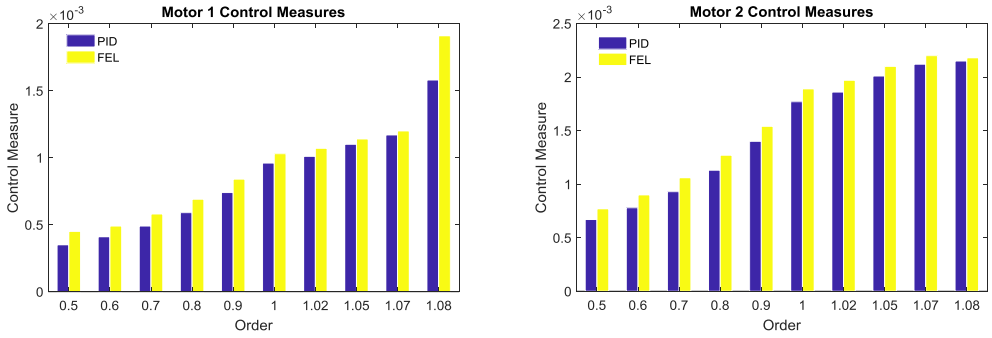

Figure 72: RMST of Motor 1 and Motor 2 with different orders

Table 9: The error measures of motor 1 with different orders

		Order				
Error Measure	Controller	0.50	0.60	0.70	0.80	0.90
ISE	PID	816.9	991.4	1223.3	1533.8	1954.5
	FEL	58.9	69.1	84.4	104.8	132.5
IAE	PID	2216.5	2453.2	2720.5	3023.0	3366.7
	FEL	542.9	578.7	612.1	658.5	734.5
ITAE	PID	1606.2	1824.1	2075.3	2365.9	2703.9
	FEL	376.8	394.6	406.8	434.0	495.8
RMSE	PID	26.5	29.3	32.5	36.1	40.2
	FEL	6.5	6.9	7.3	7.9	8.8
Error Measure	Controller	1	1.02	1.05	1.07	1.08
ISE	PID	2533.8	2674.6	2905.1	3073.0	3224.6
	FEL	172.3	182.4	199.4	212.1	320.2
IAE	PID	3760.2	3846.0	3979.5	4071.8	4076.8
	FEL	840.0	865.6	906.7	936.2	1222.9
ITAE	PID	3100.6	3188.1	3325.2	3420.8	3438.2
	FEL	589.4	612.6	650.5	678.0	814.2
RMSE	PID	44.9	46.0	47.6	48.6	48.7
	FEL	10.0	10.3	10.8	11.2	14.6

Table 10: The error measures of motor 2 with different orders

		Order				
Error Measure	Controller	0.50	0.60	0.70	0.80	0.90
ISE	PID	1546.1	1889.7	2336.2	2916.8	3673.8
	FEL	100.4	122.1	149.2	183.5	227.9
IAE	PID	3090.9	3424.9	3796.8	4210.3	4669.4
	FEL	702.6	751.8	797.2	850.8	935.4
ITAE	PID	2191.8	2493.5	2834.9	3221.0	3658.0
	FEL	484.7	509.8	527.5	552.8	613.5
RMSE	PID	36.9	40.9	45.4	50.3	55.8
	FEL	8.4	9.0	9.5	10.2	11.2
Error Measure	Controller	1	1.02	1.05	1.07	1.08
ISE	PID	4666.5	4900.2	5276.7	5546.5	5606.7
	FEL	287.3	301.8	325.6	343.2	348.7
IAE	PID	5178.6	5287.0	5453.9	5568.3	5568.7
	FEL	1059.7	1090.3	1141.2	1187.7	1216.7
ITAE	PID	4154.5	4261.7	4427.9	4542.6	4561.2
	FEL	717.5	744.1	788.7	824.9	846.1
RMSE	PID	61.9	63.2	65.2	66.5	66.6
	FEL	12.7	13.0	13.6	14.2	14.5

In this part, a detailed multibody dynamical model is used to evaluate the performances of the PID and FEL type control systems for the execution of the finger exoskeleton, namely the Exo-pinch. The proposed fractional order passive torque resistances are modeled and applied in the simulations, as well. We propose this model due to the potential of the fractional order models to model the abnormal cases. Various fractional order values are used and the performance of the controllers are evaluated. This is due to the fact that actual order is not known for the patients. We aim to estimate the passive torque values during the implementation of Exo-pinch and identify the order of the passive torque dynamics using the estimated torque values. It can be shown that using a quasi-static model and using the measurements of the applied torque input and the resulting kinematic variations, it is possible to estimate the passive

torques. As a prediction, the identified order may converge to 1 during the recovery of the patient.

Different measures are used to impose different specifications of the control system such as the transient or the steady-state responses. All measures reveal that FEL type has better performance than the PID. FEL can cope with the uncertainty due to the passive torque resistances even in case of fractional order dynamics exist. However, FEL consumes much more energy than PID. The adaptive component in the FEL type control action requires additional control energy. This is not a surprise. In the next phase, it is aimed to use fractional order artificial neural networks so as to improve the performance of the FEL controller.

The control system plays a distinctive role in the robotic rehabilitation after stroke. Such adaptive topologies are useful to reach an exact recovery. Using the tools of modeling and control, such as modeling the spasticity after stroke and modeling the cortical reorganization in the brain, opens the door to the optimal therapy which should be specific to the patient.

CHAPTER 8

QUASI-STATIC MODEL OF THE EXO-PINCH SYYSTEM

8.1 Kinetic analysis

The Exo-finger will be used for rehabilitation purpose. Due to the spasticity at the finger joints after stroke will increase the torque requirement of the actuators. The kinetical analysis is required to monitor the amount of motor torque to achieve the desired kinematics. It is assumed that the mass and the moment of inertia of the links in the Exo-finger mechanism are small. In addition, desired motion has low acceleration profiles as well. Therefore a quasi-static type of kinetical analysis is performed to find the required motor torques against the impedances at joints and the external force at the tip point K_0. Virtual work method is utilized to obtain the required actuator torques.

8.2 Velocity analysis

The velocity analysis is required to find the components of the Jacobian terms. Velocity closure equations are derived from the loop-closure equations of the loops.

Loop 1:

$$\begin{bmatrix}\dot{\theta}_3\\ \dot{\theta}_4\end{bmatrix} = \begin{bmatrix} a_3\sin(\theta_3) & -a_{42}\sin(\theta_4) - a_{41}\sin(\theta_4+\frac{\pi}{2}) \\ -a_3\cos(\theta_3) & a_{42}\cos(\theta_4) + a_{41}\cos(\theta_4+\frac{\pi}{2}) \end{bmatrix}^{-1} \begin{bmatrix} -a_2\sin(\theta_2) \\ a_2\cos(\theta_2)\end{bmatrix}\dot{\theta}_2 = \begin{bmatrix} j_1 \\ j_2\end{bmatrix}\dot{\theta}_2$$

Loop 3:

$$\begin{bmatrix}\dot{\theta}_6\\ \dot{\theta}_7\end{bmatrix}$$

$$= \begin{bmatrix} a_6\sin(\theta_6) & -a_{72}\sin(\theta_7) - a_{71}\sin(\theta_7+\frac{\pi}{2}) \\ -a_6\cos(\theta_6) & a_{72}\cos(\theta_7) + a_{71}\cos(\theta_7+\frac{\pi}{2}) \end{bmatrix}^{-1} \begin{bmatrix} -a_{41}\sin(\theta_4+\frac{\pi}{2}) + a_{42}\sin(\theta_4) & -a_5\sin(\theta_5) \\ a_{41}\cos(\theta_4+\frac{\pi}{2}) - a_{42}\cos(\theta_4) & a_5\cos(\theta_5)\end{bmatrix}\begin{bmatrix}\dot{\theta}_4\\ \dot{\theta}_5\end{bmatrix}$$

$$\begin{bmatrix}\dot{\theta}_6\\ \dot{\theta}_7\end{bmatrix} = \begin{bmatrix} j_3 & j_4 \\ j_5 & j_6\end{bmatrix}\begin{bmatrix}\dot{\theta}_4\\ \dot{\theta}_5\end{bmatrix}$$

Loop 2:

$$\begin{bmatrix}\dot{\theta}_5\\ \dot{\theta}_8\end{bmatrix}$$

$$=\begin{bmatrix} a_{51}\sin(\theta_5+\beta_2) & -a_8\sin(\theta_8)\\ -a_{51}\cos(\theta_5+\beta_2) & a_8\cos(\theta_8)\end{bmatrix}^{-1}\begin{bmatrix}-a_2\sin(\theta_2) & -a_3\sin(\theta_3) & a_9\sin(\theta_9)\\ a_2\cos(\theta_2) & a_3\cos(\theta_3) & -a_9\cos(\theta_9)\end{bmatrix}\begin{bmatrix}\dot{\theta}_2\\ \dot{\theta}_3\\ \dot{\theta}_9\end{bmatrix}$$

$$\begin{bmatrix}\dot{\theta}_5\\ \dot{\theta}_8\end{bmatrix}=\begin{bmatrix}j_7 & j_8 & j_9\\ j_{10} & j_{11} & j_{12}\end{bmatrix}\begin{bmatrix}\dot{\theta}_2\\ \dot{\theta}_3\\ \dot{\theta}_9\end{bmatrix}$$

Loop 4:

$$\begin{bmatrix}\dot{\theta}_{11}\\ \dot{\theta}_{12}\end{bmatrix}$$

$$=\begin{bmatrix} b_{42}\sin(\theta_{11})+b_{41}\sin(\theta_{11}+\frac{\pi}{2}) & -b_3\sin(\theta_{12})\\ -b_{42}\cos(\theta_{11})-b_{41}\cos(\theta_{11}+\frac{\pi}{2}) & b_3\cos(\theta_{12})\end{bmatrix}^{-1}\begin{bmatrix}-a_{72}\sin(\theta_7)+a_{71}\sin(\theta_7+\frac{\pi}{2}) & b_2\sin(\theta_{10})\\ a_{72}\cos(\theta_7)-a_{71}\cos(\theta_7+\frac{\pi}{2}) & -b_2\cos(\theta_{10})\end{bmatrix}\begin{bmatrix}\dot{\theta}_7\\ \dot{\theta}_{10}\end{bmatrix}$$

$$\begin{bmatrix}\dot{\theta}_{11}\\ \dot{\theta}_{12}\end{bmatrix}=\begin{bmatrix}j_{13} & j_{14}\\ j_{15} & j_{16}\end{bmatrix}\begin{bmatrix}\dot{\theta}_7\\ \dot{\theta}_{10}\end{bmatrix}$$

Velocity components of the tip point K_0 are required as well. The position of the tip point is given as below.

$\vec{r}_{K0}=(a_{12}-a_{11}i)+2a_{42}e^{i\theta_4}+2a_{72}e^{i\theta_7}+2b_{42}e^{i\theta_{11}}$

Taking the time derivative and resolving into the x and y components of the velocity of point K_0 give the following components.

$V_{K0\,x}=-2a_{42}\sin(\theta_4)\dot{\theta}_4-2a_{72}\sin(\theta_7)\dot{\theta}_7-2b_{42}\sin(\theta_{11})\dot{\theta}_{11}$

$V_{K0\,y}=2a_{42}\cos(\theta_4)\dot{\theta}_4+2a_{72}\cos(\theta_7)\dot{\theta}_7+2b_{42}\cos(\theta_{11})\dot{\theta}_{11}$

8.3 Virtual Work modeling

Virtual Work Theorem is utilized for modeling the mechanism, in this theorem, it is assumed that the system is at static equilibrium throughout its movement. This assumption is close to our system as the inertia of the designed Exo-pinch system is

negligible and the inertial forces are so small that the motion can be studied as quasi-static. The external torques applied on the mechanism by the motors are T_2, T_9 and, F_k is the pinching force exerted by the user on the flexible object such as a spring as shown in Figure 38, and Passive Torques (T_{MP}, T_{PIP}, T_{DIP}), which are due to the resistances of the human finger to motion on the system as shown in Figure 60. From the Virtual Work Theorem:

$$\delta W = \delta W_9 + \delta W_2 + \delta W_{MP} + \delta W_{PIP} + \delta W_{DIP} + \delta W_{F_K} = 0 \qquad (1)$$

Each term shown above are the virtual work done by external force or torques on the system, that are provided below:

$$\delta W_9 = T_9\,\delta\theta_9, \delta W_2 = T_2\,\delta\theta_2, \delta W_{MCP} = T_{MP}\,\delta\theta_4, \delta W_{PIP} = T_{PIP}\,\delta\theta_7$$

$$\delta W_{DIP} = T_{DIP}\,\delta\theta_{11}, \delta W_{F_K} = \overrightarrow{F_{K0}}.\overrightarrow{\delta r_{K0}}$$

Where:

$$\overrightarrow{F_K} = |F_{K0}|e^{i(\theta_{11}+\frac{\pi}{2})} = |F_{K0}|\left[\cos\left(\theta_{11}+\frac{\pi}{2}\right) + i\left(\sin\left(\theta_{11}+\frac{\pi}{2}\right)\right)\right] \qquad (2)$$

$$\overrightarrow{r_{K0}} = (a_{12} - a_{11}i) + 2a_{42}e^{i\theta_4} + 2a_{72}e^{i\theta_7} + 2b_{42}e^{i\theta_{11}} \qquad (3)$$

$$\delta r_{K0x} = -2a_{42}\sin(\theta_4)\delta\theta_4 - 2a_{72}\sin(\theta_7)\delta\theta_7 - 2b_{42}\sin(\theta_{11})\,\delta\theta_{11} \qquad (4)$$

$$\delta r_{K0y} = 2a_{42}\cos(\theta_4)\delta\theta_4 + 2a_{72}\cos(\theta_7)\delta\theta_7 + 2b_{42}\cos(\theta_{11})\,\delta\theta_{11} \qquad (5)$$

From equations (2), (4) and (5), virtual work term for FK0 can be written as below:

$$\delta W_{F_{K0}} = -2|F_{K0}|\cos\left(\theta_{11}+\frac{\pi}{2}\right)[a_{42}\sin(\theta_4)\delta\theta_4 + a_{72}\sin(\theta_7)\delta\theta_7 + b_{42}\sin(\theta_{11})\,\delta\theta_{11}] + 2|F_{K0}|\sin\left(\theta_{11}+\frac{\pi}{2}\right)[a_{42}\cos(\theta_4)\delta\theta_4 + a_{72}\cos(\theta_7)\delta\theta_7 + b_{42}\cos(\theta_{11})\,\delta\theta_{11}] \qquad (6)$$

Substituting all the virtual work terms in equation (1):

$$T_9\delta\theta_9 + T_2\delta\theta_2 + [T_{MCP} + |F_{K0}|.U4]\delta\theta_4 + [T_{PIP} + |F_{K0}|.U7]\delta\theta_7 + [T_{DIP} + |F_{K0}|.U11]\delta\theta_{11} = 0 \qquad (7)$$

Where $U_4, U_7\ and\ U_{11}$ are as below:

$$U_4 = 2a_{42}[\sin\left(\theta_{11}+\frac{\pi}{2}\right)\cos(\theta_4) - \cos\left(\theta_{11}+\frac{\pi}{2}\right)\sin(\theta_4)]$$

$$U_7 = 2a_{72}\left[\sin\left(\theta_{11}+\frac{\pi}{2}\right)\cos(\theta_7) - \cos\left(\theta_{11}+\frac{\pi}{2}\right)\sin(\theta_7)\right]$$

$$U_{11} = 2b_{42}[\sin\left(\theta_{11}+\frac{\pi}{2}\right)\cos(\theta_{11}) - \cos\left(\theta_{11}+\frac{\pi}{2}\right)\sin(\theta_{11})]$$

System is two degree of freedom, therefore two Independent generalized coordinates are required, which are$\delta\theta_2\ and\ \delta\theta_9$. Hence, other coordinates need to be transformed into $\delta\theta_2\ and\ \delta\theta_9$.

$$\delta\theta_4 = J_2\delta\theta_2 \qquad (8)$$

$$\delta\theta_7 = [J_5J_2 + J_6J_7 + J_6J_1J_8]\delta\theta_2 + J_9J_6\delta\theta_9 \qquad (9)$$

$$\delta\theta_{11} = \left[J_{13}[J_5J_2 + J_6J_7 + J_6J_1J_8] + J_{14}[J_3J_2 + J_4J_7 + J_4J_1J_8]\right]\delta\theta_2 + J_9(J_6J_{13} + J_{14}J_4)\delta\theta_9 \qquad (10)$$

Substituting the above equations in equation (7), the below terms would be derived:

$$[T_2 + [T_{MCP} + |F_K|.U_4]J_2 + [T_{PIP} + |F_K|.U_7][J_5J_2 + J_6J_7 + J_6J_1J_8] + [T_{DIP} + |F_K|.U_{11}]\left[J_{13}[J_5J_2 + J_6J_7 + J_6J_1J_8] + J_{14}[J_3J_2 + J_4J_7 + J_4J_1J_8]\right] = 0 \qquad (11)$$

$$T_9 + [T_{PIP} + |F_K|.U_7]J_9J_6 + [T_{DIP} + |F_K|.U_{11}]J_9(J_6J_{13} + J_{14}J_4) = 0 \qquad (12)$$

Combining equation (11) and (12), the inverse kinetics of the mechanism would be derived, which is given below.

$$\begin{bmatrix}T_2\\T_9\end{bmatrix} = -\begin{bmatrix}X_1 & X_2 & X_3 & X_4\\X_5 & X_6 & X_7 & X_8\end{bmatrix}\begin{bmatrix}T_{MCP}\\T_{PIP}\\T_{DIP}\\|F_{K0}|\end{bmatrix} \qquad (13)$$

X_1 Through X_8 are given as follows:

$$X_1 = J_2$$

$$X_2 = J_5J_2 + J_6J_7 + J_6J_1J_8$$

$$X_3 = \left[J_{13}[J_5J_2 + J_6J_7 + J_6J_1J_8] + J_{14}[J_3J_2 + J_4J_7 + J_4J_1J_8]\right]$$

$$X_4 = U11\left[J_{13}[J_5J_2 + J_6J_7 + J_6J_1J_8] + J_{14}[J_3J_2 + J_4J_7 + J_4J_1J_8]\right] + J_2U4 + U7[J_5J_2 + J_6J_7 + J_6J_1J_8]$$

$$X_5 = 0$$

$$X_6 = J_9J_6$$

$$X_7 = J_9(J_6J_{13} + J_{14}J_4)$$

$$X_8 = U11 \cdot J_9(J_6J_{13} + J_{14}J_4) + \mathrm{U7} \cdot J_9J_6$$

Direct kinetics given below:

$$\begin{bmatrix}X_1 & X_2 & X_3\\0 & X_6 & X_7\end{bmatrix}\begin{bmatrix}T_{MCP}\\T_{PIP}\\T_{DIP}\end{bmatrix} = -\begin{bmatrix}T_{A_0} + |F_{K0}|X_4\\T_{H_0} + |F_{K0}|X_8\end{bmatrix} \qquad (14)$$

8.4 Estimation of passive torques

Passive torques on any individual is different form the other. In [paper for passive torques], passive torques are characterized as below, which is dependent of the angular speed and position of the joint:

$$\tau_i = B_i\dot{\theta}_\iota + K_i(\theta_i)\,\Delta\theta_i \quad (15)$$

Where (τ_i) is the corresponding passive torque, and $\Delta\theta_i$ is different of current position with the position 50ms earlier. B is a constant and K is function of angular position that is given below;

$$K_i = K_{i1}\theta^2 + K_{i2}\theta + K_{i3} \qquad (16)$$

The above equations are written based on the assumptions that inertias and static passive torques are negligible.

These constant are different for different individuals and during the process; it is highly required to estimate these in order to obtain passive torques. This process is crucial, as corresponding motor torques can be obtained from equations (13). Equation (14) is underdetermined; therefore it is not possible to find the characteristics, however, by designing specific patterns, it is possible to keep corresponding joints responsible constant through the process, which would result in zero passive torques in that joint, as it can be seen in equation (15).

Two scenarios are considered for finding the characteristics of the passive torques for any person. First of all, a pattern would be given to system that keeps the MCP joint constant, which means MCP passive torque is zero. Secondly, PIP and DIP joints would remain constant throughout the motion. The scenarios are explains in detail in the following paragraphs in the case that motor cases are given previously.

First scenario:

If MCP joint is fixed, then its corresponding passive torque is also zero, as it can be seen from equation (15), this helps transforming the equation (14), which now it is possible to find the passive torques:

$$\begin{bmatrix} X_2 & X_3 \\ X_6 & X_7 \end{bmatrix}\begin{bmatrix} T_{PIP} \\ T_{DIP} \end{bmatrix} = -\begin{bmatrix} T_{A_0} + |F_{K0}|X_4 \\ T_{H_0} + |F_{K0}|X_8 \end{bmatrix} \qquad (17)$$

There are four unknowns for each of the passive torques, which after finding the passive torques from equation (17), they can be found by solving equation (15) and (16) with least square method, for set of data that obtained.

Second scenario:

Now if PIP and DIP joints be fixed, there are no torques on those joints and the equation (14) is reduced to very simple equation, which helps to find the characteristics at joint MCP. However, th11, th7 and th4 are having the same angles and always going to be same through the process, this would make the DIP and PIP always at 180 degrees.

$$X_1 T_{MCP} = -T_{A_0} - F_0 X_4 \qquad (18)$$

With the same process that explained for first scenario, coefficients would be obtained for MCP joint.

8.5 Required tests

Three set of experiments are designed for proving the mentioned concepts.

Using the given pattern for both scenarios and previously found characteristics in [21], the required motor torques are obtained from equation (13), Which later used with kinematics of the mechanism to find the passive torques from equations (17) and (18) in each scenario. Gaussian noise would be given to motor torques obtained from equation (13) and used for finding the coefficients of the joints. This would help us see the differences caused by possible noises in real systems.

The same pattern would be given to mechanism available in Simmechanics. The required torques for mechanism would be compared to the one obtained from Virtual Work theorem equations. This would prove the assumptions made in VW method are to what extend reliable.

8.6 Analysis and tests

For proving the concepts that explained in previous part, a set of experiments are designed. Coefficients for calculating the passive torques of index finger were taken from Table 7 and Table 8 and these were used to find the required motor torques for performing desired patterns in both SimMechanics Model and VW model.

Three Different Pattern were utilized for study purposes, the first pattern is called full pattern as all of the finger's joints are moving and complete pinching motion. In second patter, MCP joint is kept fixed, and in last pattern, only MCP joint is moving and PIP and DIP joint is kept fixed.

Pattern 1: This pattern is for performing pinching motion, Motor angles, and all the joints angles are provided in Figure 73.

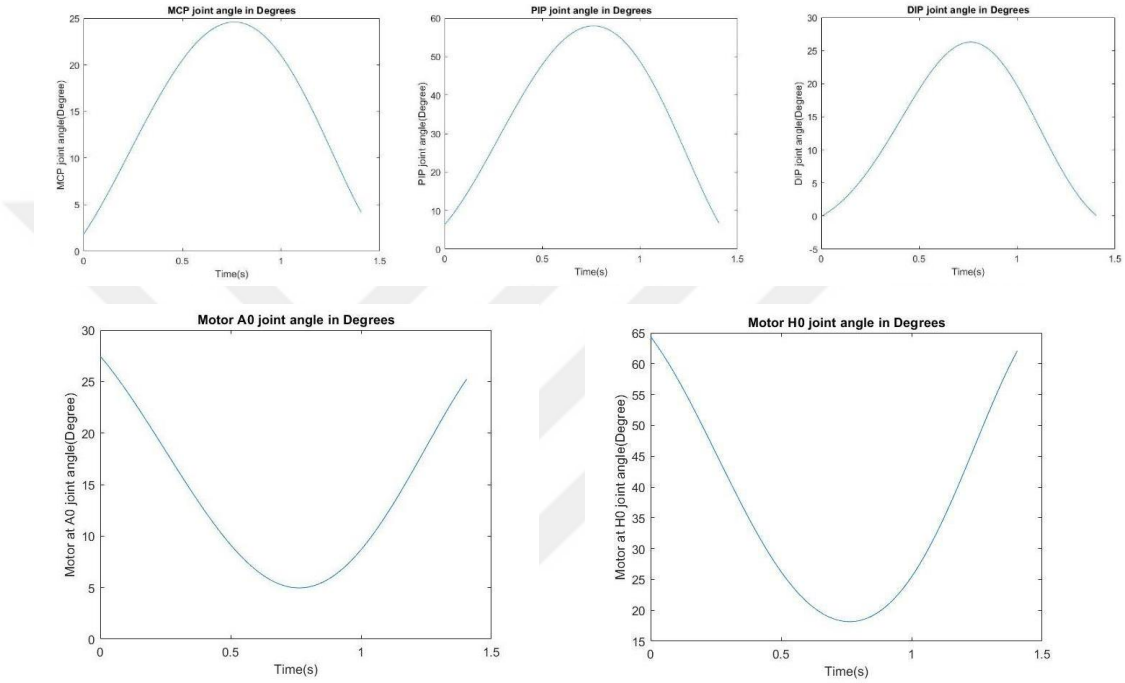

Figure 73: Pattern 1 for performing full pinching motion

Pattern 2: MCP angle is kept fixed at zero-degree, PIP and DIP joints move. The motor angles and joint angles are provided in Figure 74.

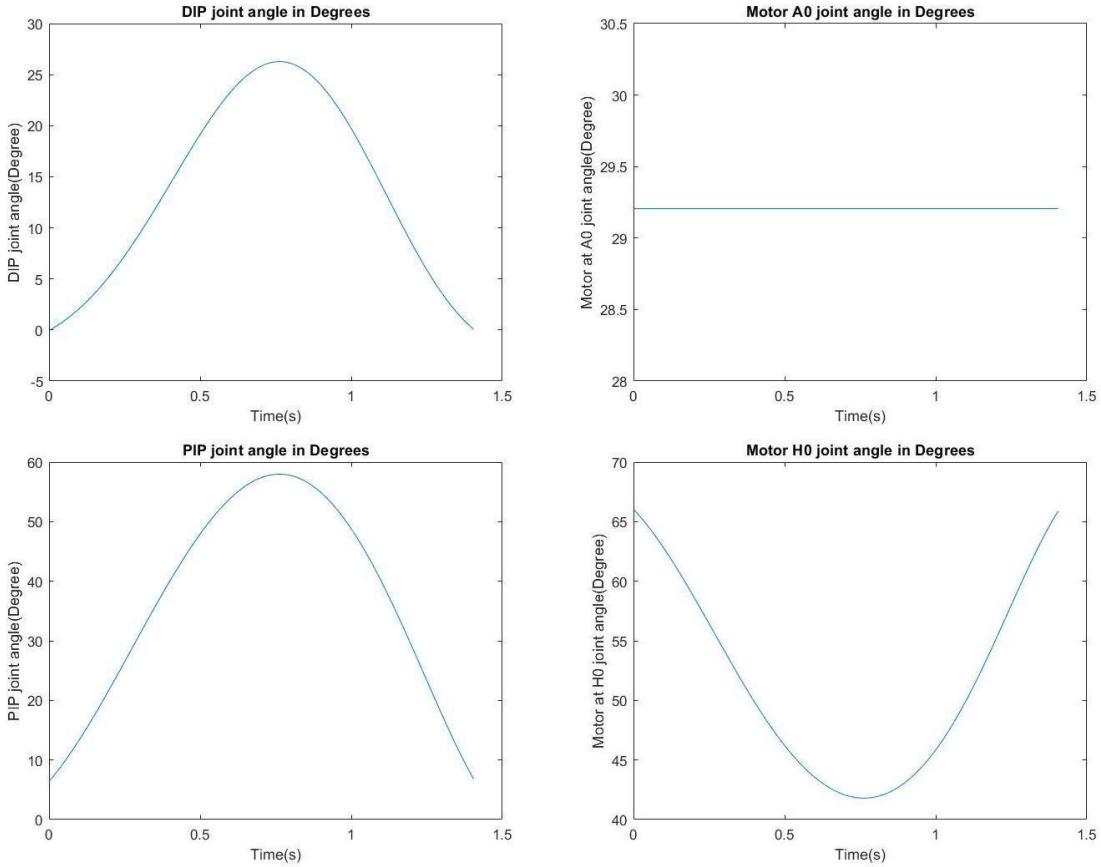

Figure 74: MCP angle is kept fixed at zero-degree, PIP and DIP joints move

Pattern 3: DIP and PIP angles are zero degree throughout the motion and only MCP moves. Motor angles and MCP angle is given in Figure 75.

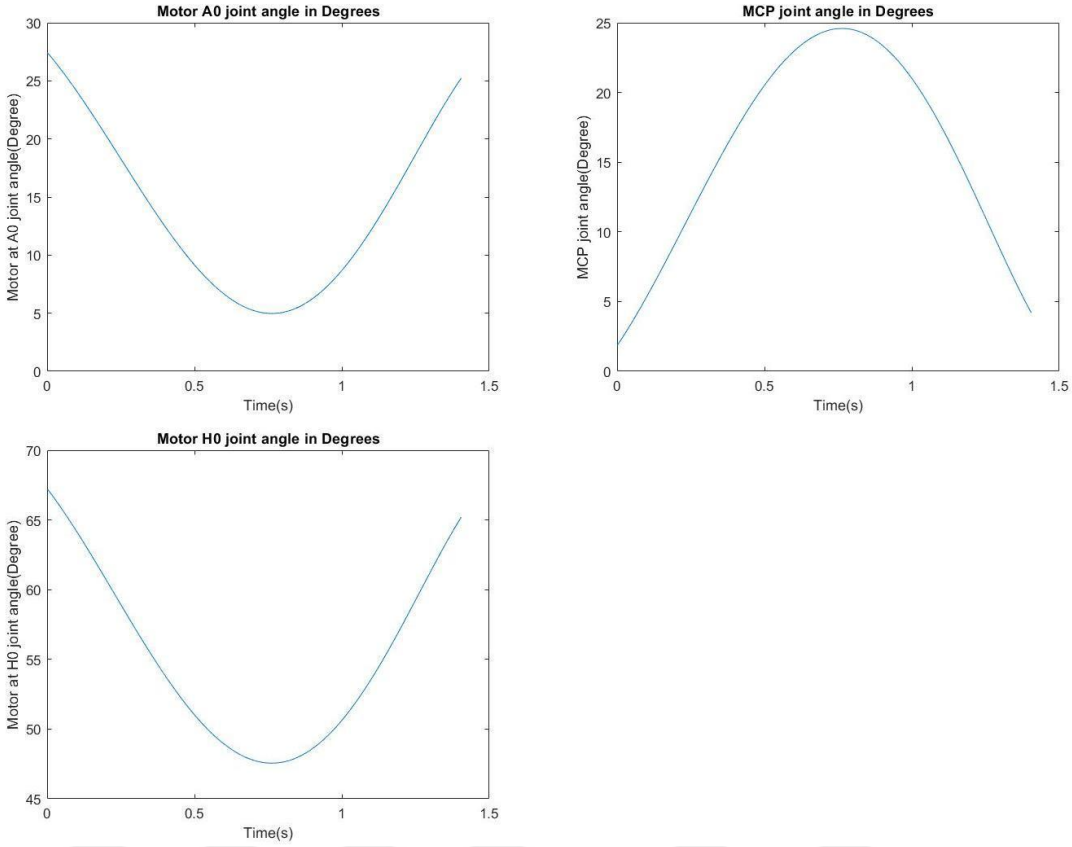

Figure 75: DIP and PIP angles are fixed at zero degree and only MCP moves

8.7 Comparisons based on simulation

All the mentioned patterns were ran on Sim-Mechanics model, with an external pinching force applied on index finger tip, shown in Figure 76, and motor torques are taken form, as an example to prove this concept. The patterns of pinching motion is performed under 2 seconds, which causes the inertia forces to be more effective. Same patterns were used in virtual work model and the corresponding torques were obtained for comparison purposes.

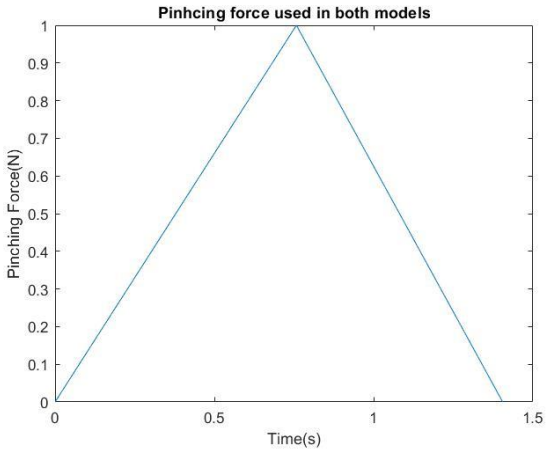

Figure 76: Spring type external force

This external force starts from zero N at natural position of index finger and increases to the maximum of 1 N during flexion motion, then goes back to zero during extension motion.

For the pattern 1, 2 and 3 the torques obtained for both models are given in Figure 77, Figure 78 and Figure 79 consequently.

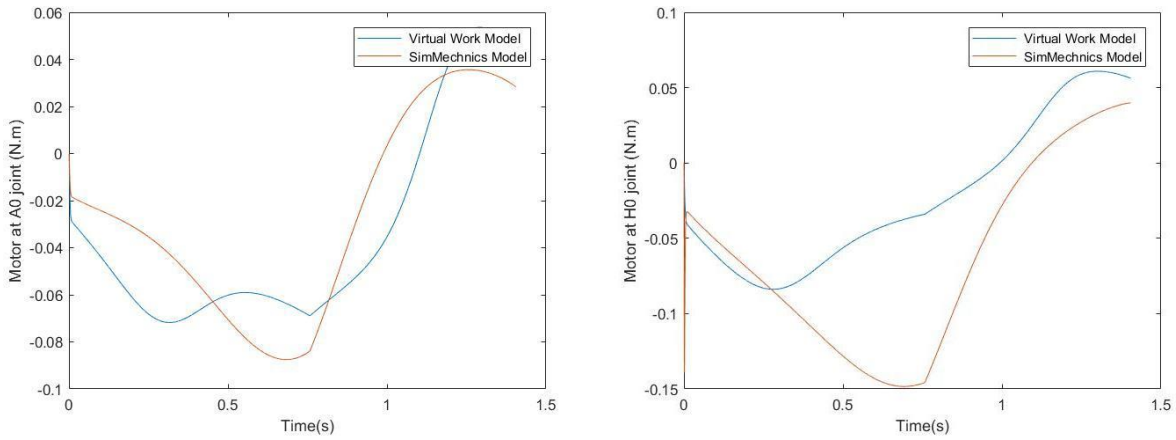

Figure 77: Motor torque comparison for pattern 1

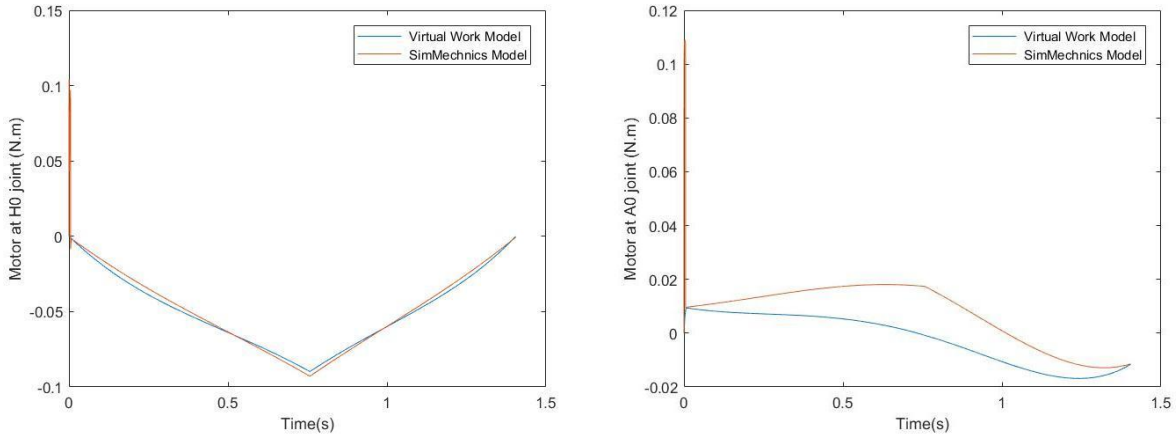

Figure 78: Motor torque comparison for pattern 2

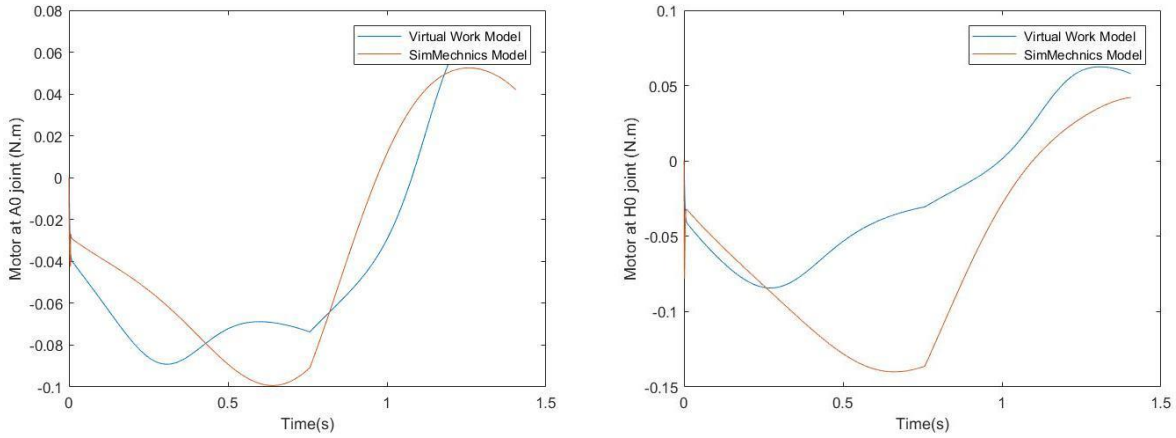

Figure 79: Motor torque comparison for pattern 3

As a result we can say that both Sim-Mechanics model and VW model models approximately give us the same results. It is a kind of validation of VW model as a kinetic model and Sim-Mechanics model designed based on kinematic approach. It is important for us, because we plan to use kinetic model to estimate petitions fingers spasticity and design a torque on demand controller for our system.

CHAPTER 9

CONCLUSIONS

The main motivation of this thesis is to design an exoskeleton system for robotic mirror therapy, in a way that the system exerts sufficient perpendicular forces on the finger phalanges safely to perform pinching motion by the index and thumb fingers.

To design such a system, it is not only enough to consider mechanical parameters such as systems' kinematic, the actuating method, power transmission system and controller structure but also we should consider biomechanical characteristics of system. Considering these multidisciplinary issues, we designed and manufactured the Exo-pinch mechanism with totally 4-DOF; one for extension/flexion of the thumb and two for extension/flexion of index finger, and the 1-DOF is used to do the abduction-adduction motion of the thumb finger. The mechanism links were fabricated from high strength Aluminum metal. The selected actuators were two 24 V DC electrical motors and two servo motors which are controlled in Simulink Desktop Real-Time environment by using the Humusoft Data Acquisition board.

The advantage of this prototype is that, the position control can be applied together with the torque control during pinching. At the same time, we can estimate the passive torques applied on the index finger joints. Another advantage of this prototype is that the abduction/adduction motion of the thumb finger is controlled, so the executed pinching motion is more realistic.

The Exo-pinch mechanism was tested on the hand of healthy people and patients for several times. The results were valuable for the future studies. In the multi-objective optimization process, using optimal solutions may provide more compact designs. Ergonomic issues should be considered for the future versions. Hybrid control architecture composed of low-level adaptive control architectures will be applied on patients with the revised versions of Exo-Pinch.

REFERENCES

[1] R. T. Lauer, K. L. Kilgore, P. H. Peckham, N. Bhadra, and M. W. Keith, "The function of the finger intrinsic muscles in response to electrical stimulation," *Rehabilitation Engineering, IEEE Transactions on,* vol. 7, no. 1, pp. 19-26, 1999.

[2] J. M. Heasman *et al.*, "Detection of fatigue in the isometric electrical activation of paralyzed hand muscles of persons with tetraplegia," *Rehabilitation Engineering, IEEE Transactions on,* vol. 8, no. 3, pp. 286-296, 2000.

[3] D. Jack *et al.*, "Virtual reality-enhanced stroke rehabilitation," *Neural Systems and Rehabilitation Engineering, IEEE Transactions on,* vol. 9, no. 3, pp. 308-318, 2001.

[4] C. G. Burgar, P. S. Lum, P. C. Shor, and H. M. Van der Loos, "Development of robots for rehabilitation therapy: the Palo Alto VA/Stanford experience," *Journal of rehabilitation research and development,* vol. 37, no. 6, pp. 663-674, 2000.

[5] N. Petroff, K. D. Reisinger, and P. A. Mason, "Fuzzy-control of a hand orthosis for restoring tip pinch, lateral pinch, and cylindrical prehensions to patients with elbow flexion intact," *Neural Systems and Rehabilitation Engineering, IEEE Transactions on,* vol. 9, no. 2, pp. 225-231, 2001.

[6] K. L. Kilgore, R. T. Lauer, and P. H. Peckham, "A transducer for the measurement of finger joint moments," *Rehabilitation Engineering, IEEE Transactions on,* vol. 6, no. 4, pp. 424-429, 1998.

[7] G. J. Byers, B. S. Goldstein, and J. E. Sanders, "An electromechanical testing device for assessment of hand motor function," *Rehabilitation Engineering, IEEE Transactions on,* vol. 6, no. 1, pp. 88-94, 1998.

[8] H. Yamaura, K. Matsushita, R. Kato, and H. Yokoi, "Development of hand rehabilitation system for paralysis patient–universal design using wire-driven mechanism–," in *Engineering in Medicine and Biology Society, 2009. EMBC*

2009. Annual International Conference of the IEEE, 2009, pp. 7122-7125: IEEE.

[9] A. Wege and G. Hommel, "Development and control of a hand exoskeleton for rehabilitation of hand injuries," in *Intelligent Robots and Systems, 2005.(IROS 2005). 2005 IEEE/RSJ International Conference on*, 2005, pp. 3046-3051: IEEE.

[10] H. Kawasaki *et al.*, "Development of a hand motion assist robot for rehabilitation therapy by patient self-motion control," in *Rehabilitation Robotics, 2007. ICORR 2007. IEEE 10th International Conference on*, 2007, pp. 234-240: IEEE.

[11] M. Mulas, M. Folgheraiter, and G. Gini, "An EMG-controlled exoskeleton for hand rehabilitation," in *Rehabilitation Robotics, 2005. ICORR 2005. 9th International Conference on*, 2005, pp. 371-374: IEEE.

[12] M. DiCicco, L. Lucas, and Y. Matsuoka, "Comparison of control strategies for an EMG controlled orthotic exoskeleton for the hand," in *Robotics and Automation, 2004. Proceedings. ICRA'04. 2004 IEEE International Conference on*, 2004, vol. 2, pp. 1622-1627: ieee.

[13] A. Chiri *et al.*, "HANDEXOS: Towards an exoskeleton device for the rehabilitation of the hand," in *Intelligent Robots and Systems, 2009. IROS 2009. IEEE/RSJ International Conference on*, 2009, pp. 1106-1111: IEEE.

[14] I. H. Ertas, E. Hocaoglu, D. E. Barkana, and V. Patoglu, "Finger exoskeleton for treatment of tendon injuries," in *Rehabilitation Robotics, 2009. ICORR 2009. IEEE International Conference on*, 2009, pp. 194-201: IEEE.

[15] M. Fontana, A. Dettori, F. Salsedo, and M. Bergamasco, "Mechanical design of a novel hand exoskeleton for accurate force displaying," in *Robotics and Automation, 2009. ICRA'09. IEEE International Conference on*, 2009, pp. 1704-1709: IEEE.

[16] H. Fang, Z. Xie, and H. Liu, "An exoskeleton master hand for controlling DLR/HIT hand," in *Intelligent Robots and Systems, 2009. IROS 2009. IEEE/RSJ International Conference on*, 2009, pp. 3703-3708: IEEE.

[17] P. Stergiopoulos, P. Fuchs, and C. J. E. Laurgeau, Dublin, Ireland, "Design of a 2-finger hand exoskeleton for VR grasping simulation," pp. 80-93, 2003.

[18] Y. Hasegawa, Y. Mikami, K. Watanabe, and Y. Sankai, "Five-fingered assistive hand with mechanical compliance of human finger," in *Robotics and Automation, 2008. ICRA 2008. IEEE International Conference on*, 2008, pp. 718-724: IEEE.

[19] M. J. Lelieveld, T. Maeno, and T. Tomiyama, "Design and development of two concepts for a 4 DOF portable haptic interface with active and passive multi-point force feedback for the index finger," in *ASME 2006 International Design Engineering Technical Conferences and Computers and Information in Engineering Conference*, 2006, pp. 547-556: American Society of Mechanical Engineers.

[20] H. Kawasaki, H. Kimura, S. Ito, Y. Nishimoto, H. Hayashi, and H. Sakaeda, "Hand rehabilitation support system based on self-motion control, with a clinical case report," in *Automation Congress, 2006. WAC'06. World*, 2006, pp. 1-6: IEEE.

[21] D. G. Kamper, T. G. Hornby, and W. Z. Rymer, "Extrinsic flexor muscles generate concurrent flexion of all three finger joints," *Journal of biomechanics,* vol. 35, no. 12, pp. 1581-1589, 2002.

[22] Y. A. Gandomi, "Modeling the index finger of a clinician during the course of physical exam," 2012.

[23] M. Lelieveld and T. Maeno, "Design and development of a 4 DOF portable haptic interface with multi-point passive force feedback for the index finger," in *Robotics and Automation, 2006. ICRA 2006. Proceedings 2006 IEEE International Conference on*, 2006, pp. 3134-3139: IEEE.

[24] Z. Tang, S. Sugano, and H. Iwata, "A finger exoskeleton for rehabilitation and brain image study," in *Rehabilitation Robotics (ICORR), 2013 IEEE International Conference on*, 2013, pp. 1-6: IEEE.

[25] J. Iqbal, N. Tsagarakis, and D. Caldwell, "Design of a wearable direct-driven optimized hand exoskeleton device," in *The Fourth International Conference*

on Advances in Computer-Human Interactions (ACHI), Gosier, Guadeloupe, France, Feb, 2011, pp. 23-28: Citeseer.

[26] J. Iqbal, H. Khan, N. G. Tsagarakis, and D. G. Caldwell, "A novel exoskeleton robotic system for hand rehabilitation–Conceptualization to prototyping," *Biocybernetics and biomedical engineering*, vol. 34, no. 2, pp. 79-89, 2014.

[27] A. E. Fiorilla, F. Nori, L. Masia, and G. Sandini, "Finger impedance evaluation by means of hand exoskeleton," *Annals of biomedical engineering*, vol. 39, no. 12, pp. 2945-2954, 2011.

[28] P. Agarwal and A. D. Deshpande, "Impedance and force-field control of the index finger module of a hand exoskeleton for rehabilitation," in *Rehabilitation Robotics (ICORR), 2015 IEEE International Conference on*, 2015, pp. 85-90: IEEE.

[29] K. Russell, Q. Shen, and R. S. Sodhi, *Mechanism Design: Visual and Programmable Approaches*. CRC Press, 2013.

[30] G. A. Hassaan, M. A. Al-Gamil, and M. M. Lashin, "New Approach for the Synthesis of Planar 4-Bar Mechanisms for 2 Coupler-Positions Generation," *New York Science Journal*, vol. 5, no. 10, pp. 86-90, 2012.

[31] A. E. Fiorilla, F. Nori, L. Masia, and G. J. A. o. b. e. Sandini, "Finger impedance evaluation by means of hand exoskeleton," vol. 39, no. 12, p. 2945, 2011.

[32] J. Iqbal, H. Khan, N. G. Tsagarakis, D. G. J. B. Caldwell, and b. engineering, "A novel exoskeleton robotic system for hand rehabilitation–conceptualization to prototyping," vol. 34, no. 2, pp. 79-89, 2014.

[33] J. Iqbal, N. G. Tsagarakis, and D. G. Caldwell, "Design of a wearable direct-driven optimized hand exoskeleton device," in *4th International Conference on Advances in Computer-Human Interactions (ACHI)*, 2011, pp. 142-146: Citeseer.

[34] E. Söylemez, *Mechanisms*. Middle East Technical University, 1979.

[35] A. R. Conn, N. I. Gould, and P. J. S. J. o. N. A. Toint, "A globally convergent augmented Lagrangian algorithm for optimization with general constraints and simple bounds," vol. 28, no. 2, pp. 545-572, 1991.

[36] A. Conn, N. Gould, and P. J. M. o. C. o. t. A. M. S. Toint, "A globally convergent Lagrangian barrier algorithm for optimization with general inequality constraints and simple bounds," vol. 66, no. 217, pp. 261-288, 1997.

[37] F. Girosi and T. J. B. c. Poggio, "Networks and the best approximation property," vol. 63, no. 3, pp. 169-176, 1990.

[38] S. Haykin, *Neural networks: a comprehensive foundation*. Prentice Hall PTR, 1994.

[39] G. Campa, M. L. Fravolini, and M. Napolitano, "A library of adaptive neural networks for control purposes," in *Computer Aided Control System Design, 2002. Proceedings. 2002 IEEE International Symposium on*, 2002, pp. 115-120: IEEE.

[40] T. Rajaee, S. A. Mirbagheri, M. Zounemat-Kermani, and V. J. S. o. t. t. e. Nourani, "Daily suspended sediment concentration simulation using ANN and neuro-fuzzy models," vol. 407, no. 17, pp. 4916-4927, 2009.

[41] J. Principe, W. Lefebvre, G. Lynn, C. Fancourt, and D. Wooten, "NeuroSolutions-Documentation, the Manual and On-Line Help," ed: Version, 2007.

[42] A. Singh, M. Imtiyaz, R. Isaac, and D. J. A. W. M. Denis, "Comparison of soil and water assessment tool (SWAT) and multilayer perceptron (MLP) artificial neural network for predicting sediment yield in the Nagwa agricultural watershed in Jharkhand, India," vol. 104, pp. 113-120, 2012.

[43] A. Tepljakov, "FOMCON: Fractional-Order Modeling and Control Toolbox," in *Fractional-order Modeling and Control of Dynamic Systems*: Springer, 2017, pp. 107-129.

[44] Y. Chen, I. Petras, and D. Xue, "Fractional order control-a tutorial," in *American Control Conference, 2009. ACC'09.*, 2009, pp. 1397-1411: IEEE.

[45] C. A. Monje, Y. Chen, B. M. Vinagre, D. Xue, and V. Feliu-Batlle, *Fractional-order systems and controls: fundamentals and applications*. Springer Science & Business Media, 2010.

[46] B. Vinagre, I. Podlubny, A. Hernandez, V. J. F. c. Feliu, and a. analysis, "Some approximations of fractional order operators used in control theory and applications," vol. 3, no. 3, pp. 231-248, 2000.

[47] A. Oustaloup, F. Levron, B. Mathieu, F. M. J. I. T. o. C. Nanot, S. I. F. Theory, and Applications, "Frequency-band complex noninteger differentiator: characterization and synthesis," vol. 47, no. 1, pp. 25-39, 2000.

[48] Y. Chen and D. P. Atherton, *Linear feedback control: analysis and design with MATLAB*. Siam, 2007.